



HAL
open science

Dynamic stiffness method: New Levy's series for orthotropic plate elements with natural boundary conditions

K. Khlifi, Jean-Baptiste Casimir, A. Akrouf, M. Haddar

► To cite this version:

K. Khlifi, Jean-Baptiste Casimir, A. Akrouf, M. Haddar. Dynamic stiffness method: New Levy's series for orthotropic plate elements with natural boundary conditions. *Engineering Structures*, 2021, 245, pp.112936. 10.1016/j.engstruct.2021.112936 . hal-03836843

HAL Id: hal-03836843

<https://hal.science/hal-03836843>

Submitted on 22 Aug 2023

HAL is a multi-disciplinary open access archive for the deposit and dissemination of scientific research documents, whether they are published or not. The documents may come from teaching and research institutions in France or abroad, or from public or private research centers.

L'archive ouverte pluridisciplinaire **HAL**, est destinée au dépôt et à la diffusion de documents scientifiques de niveau recherche, publiés ou non, émanant des établissements d'enseignement et de recherche français ou étrangers, des laboratoires publics ou privés.



Distributed under a Creative Commons Attribution - NonCommercial 4.0 International License

1
2
3
4
5
6
7
8
9
10
11
12
13
14
15
16
17
18
19
20
21
22
23
24
25
26
27
28
29
30
31
32
33
34
35
36
37
38
39
40
41
42
43
44
45
46
47
48
49
50
51
52
53
54
55
56
57
58
59
60
61
62
63
64
65

Dynamic Stiffness Method: new Levy's series for orthotropic plate elements with natural boundary conditions

K. Khelif^{a,b}, J.B. Casimir^{a,*}, A. Akrou^b, M. Haddar^b

^a*SUPMECA, EA 7393 QUARTZ Laboratory, 3 Fernand Hainaut Street, 93407, Saint-Ouen, France*

^b*ENIS, LA2MP laboratory, Sfax University, Soukra Km 3.5, BP 1173 3038 Sfax, Tunisia*

Abstract

A novel Lévy series for developing a dynamic stiffness matrix for a completely free orthotropic Kirchhoff plate is presented in this paper. The bending behavior is based on the Kirchhoff-Love thin-plate theory. The dynamic stiffness matrix is derived using the new Lévy series without classical symmetry decomposition, simplifying the building procedure. Harmonic responses obtained by this method and the finite element method are compared to establish the rate of convergence and the degree of precision of the current formulation.

Key words: Dynamic stiffness method, Lévy series, Harmonic response,

Orthotropic plate

1. Introduction

Since the advent of composite materials in structural engineering, the dynamic bending of orthotropic rectangular plates has been studied extensively. Composite materials are becoming increasingly important in aerospace, automo-

*Corresponding author

Email address: jean-baptiste.casimir@supmeca.fr (J.B. Casimir)

1
2
3
4
5
6
7
8
9
10
11
12
13
14
15
16
17
18
19
20
21
22
23
24
25
26
27
28
29
30
31
32
33
34
35
36
37
38
39
40
41
42
43
44
45
46
47
48
49
50
51
52
53
54
55
56
57
58
59
60
61
62
63
64
65

5 tive, marine, and civil engineering designs. The finite element method (FEM)
is effective for calculating the dynamic response and modal characteristics of
such structures, but limitations arise when the mode density increases. The
precision of the results is highly dependent on the mesh size, and convergence
studies must be conducted. The mesh size of finite elements depends on the
10 highest frequency in the analysis; increasing the number of finite elements re-
quires greater computational time and effort to solve the problem.

To overcome these difficulties, several meshless methods have been devel-
oped, including the dynamic stiffness method (DSM) [1] and the spectral ele-
15 ment method (SEM) [2]. These methods are fundamentally based on the exact
closed-form solution of the governing differential equations of motion. Con-
sequently, the DSM is based on the minimization of the discretization of the
structure geometry. This approach was developed extensively for beam ele-
ments in the late 20th century [3-9].

20 The extension of the meshless method to plate elements is difficult. The
main challenge is that no closed-form solution exists for the governing differen-
tial equations of motion. Even so, during the last twenty years, DSM formula-
tions for plate elements have been developed. Kim and Lee recently published
25 a paper that presents a complete survey of plate DSM formulations [10]. The
concept is based on the series development of strong solutions of the equations
of motion. This concept is not new; the first scientists to obtain strong solutions

1
2
3
4
5
6
7
8
9
10
11
12
13
14
15
16
17
18
19
20
21
22
23
24
25
26
27
28
29
30
31
32
33
34
35
36
37
38
39
40
41
42
43
44
45
46
47
48
49
50
51
52
53
54
55
56
57
58
59
60
61
62
63
64
65

based on series for the static deflection of rectangular plates were Henri Navier at the beginning of the 19th century and Maurice Lévy at the end of the 19th century. Navier used double trigonometric Fourier series to transform the partial derivative equations into an algebraic system of equations, but the boundary conditions were limited to the fully simply-supported case. Lévy used a single series built with products of trigonometric functions along one dimension and solutions of the resulting differential equation along the other dimension. The Lévy solutions are limited to plates for which two opposite edges are simply supported. Plates subject to such boundary conditions are often called Lévy plates. In the context of meshless methods and powerful computational resources, many researchers have presented new perspectives on the Navier-type and Lévy-type solutions to address static deflection, buckling, and the dynamic analysis of plates. Following the work of Langley [11] devoted to stiffened plates, the first textbook describing DSM, including Lévy-plate formulations, was written by Leung in 1993 [12]. Leung provided an exhaustive presentation of the DSM beam and Lévy-plate elements developed until the beginning of the 1990s. In the 1990s, some DSM Lévy-plate formulations were described by other authors. Bercin addressed orthotropic Lévy-plate DSM elements [13], Bercin and Langley investigated the problem of assembling non-coplanar Lévy-plate DSM elements with in-plane vibrations [14], and Leung and Zhou studied laminated composite plates [15]. However, to formulate a DSM plate element supporting connections with another coplanar or non-coplanar DSM plate along any of its four edges, solutions for fully natural boundary conditions are required. With

1
2
3
4
5
6
7
8
9
10
11
12
13
14
15
16
17
18
19
20
21
22
23
24
25
26
27
28
29
30
31
32
33
34
35
36
37
38
39
40
41
42
43
44
45
46
47
48
49
50
51
52
53
54
55
56
57
58
59
60
61
62
63
64
65

this type of solution, the resulting elementary dynamic stiffness matrices can be assembled to form a structural dynamic stiffness matrix in the same way as in the finite element method. Approximate solutions have been described by many authors in the modal analysis of rectangular plates subjected to fully natural boundary conditions, that is, with four free edges. These boundary conditions are known as “free-free-free-free” (FFFF). Leissa [16, 17] provided an extensive survey of approximate eigensolutions for the FFFF case. The approximate solutions for these boundary conditions are based on a series built with beam eigenfunctions and a Rayleigh–Ritz procedure. Gorman [18] subsequently described a superposition method to address the free vibrations of an FFFF plate with any degree of accuracy. His method superimposed two accurate Lévy solutions to exactly satisfy both FFFF boundary conditions and the symmetry properties of the modes. Each doubly symmetric, doubly antisymmetric, and antisymmetric-symmetric eigenmode is broken into two Lévy-type building blocks, for which an exact Lévy solution is used. Thus, any degree of accuracy can be obtained. In 2005, using the Gorman decomposition, Casimir et al. [19] were the first researchers to describe a DSM rectangular plate with fully natural boundary conditions. The procedure consisted of processing four dynamic stiffness matrices related to the symmetry contributions; a matricial operation was described to combine the four matrices into a complete dynamic stiffness matrix. While this DSM formulation, including natural boundary conditions, had the ability to support any other plate connection, these first works were limited to Kirchhoff’s isotropic rectangular plates. However, formulations of Lévy-plate

1
2
3
4
5
6
7
8
9
10
11
12
13
14
15
16
17
18
19
20
21
22
23
24
25
26
27
28
29
30
31
32
33
34
35
36
37
38
39
40
41
42
43
44
45
46
47
48
49
50
51
52
53
54
55
56
57
58
59
60
61
62
63
64
65

elements and other plate theories were included. In 2011, Boscolo and Banerjee described DSM Lévy plates including a first-order shear deformation theory [20] and in-plane stiffness [21]. Soon after, they described a composite Mindlin DSM Lévy plate [22, 23]. Higher-order shear deformation theory devoted to laminates was reported by Fazzolari et al. [24] in a DSM Lévy-plate formulation. DSM formulations with fully natural boundary conditions are the focus of most recent research. In 2015, the Gorman decomposition of the four symmetry contributions was used again to describe DSM plate elements. In 2015, such formulations concerning isotropic rectangular plates were reported by Banerjee et al. [25] for transverse vibrations, by Nefovska-Danilović and Petronijević [26] for in-plane vibrations, and by Kolarević et al. [27] for the Mindlin shear theory. Ghorbel et al. described an orthotropic rectangular DSM plate [28]. In 2016, extension of the Gorman decomposition to in-plane vibration was used by Ghorbel et al. [29] to describe an in-plane DSM orthotropic plate with fully natural boundary conditions. A DSM element including higher-order shear deformation effects was described by Kolarević et al. [30]. A DSM sandwich plate element was developed by Marjanović et al. [31] for fully natural boundary conditions. Many other formulations of DSM plate elements are still in progress. In 2017, Damnjanović et al. studied stiffened composite plates [32, 33] and Nefovska-Danilović et al. studied multilayered plates [34, 35] for fully natural boundary conditions. In 2018 and 2019, Kumar et al. described a Lévy-plate DSM element including functionally graded material [36, 37]. Papkov and Banerjee studied an orthotropic Mindlin plate for fully natural boundary conditions [38].

1
2
3
4
5
6
7
8
9
10
11
12
13
14
15
16
17
18
19
20
21
22
23
24
25
26
27
28
29
30
31
32
33
34
35
36
37
38
39
40
41
42
43
44
45
46
47
48
49
50
51
52
53
54
55
56
57
58
59
60
61
62
63
64
65

In the current study, a new Lévy series is defined to simplify the classical superposition approach based on symmetry decomposition. The classical approach implies eight Lévy series, and has been used since 2005 for DSM plate formulation with natural boundary conditions [19, 25, 34]. The new formulation is based on the extended Lévy series and the projection method on boundaries. Only four series are required to build the entire dynamic stiffness matrix. The use of symmetry contributions is no longer necessary, which simplifies the DSM plate formulations without a loss of accuracy. This general solution was used in 2021 for DSM formulation by Wei et al. [39] and a spectral element model by Kim and Lee [10] for isotropic plates. Numerical examples are presented for an orthotropic DSM rectangular Kirchhoff plate element. The accuracy of the formulation and the results were compared with results obtained using the finite element method (FEM).

2. Governing equations of the orthotropic rectangular plate

2.1. Plate geometry and Kirchhoff's hypothesis

The geometry of the plate is defined in a Cartesian coordinate system. Figure 1 shows an orthotropic rectangular plate defined by a thickness h and lateral dimensions $2a \times 2b$. The origin O of the Cartesian coordinate system is chosen at the center of the mid-plane of the plate, with the z -axis normal to this plane.

Kirchhoff's hypothesis is adopted; a straight line normal to the mid-surface

1
2
3
4
5
6
7
8
9
10
11
12
13
14
15
16
17
18
19
20
21
22
23
24
25
26
27
28
29
30
31
32
33
34
35
36
37
38
39
40
41
42
43
44
45
46
47
48
49
50
51
52
53
54
55
56
57
58
59
60
61
62
63
64
65

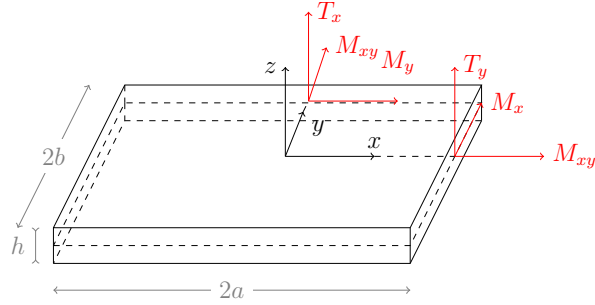


Figure 1: Geometry of the plate

of the plate remains perpendicular after deformation. Thus, the displacement
 120 at any point $M(x, y, z)$ of the volume is given by Eqs. 1. The orthotropic axes
 of the material are parallel to the x and y axes.

$$\begin{cases} u(x, y, z, t) = -z \frac{\partial W}{\partial x} \\ v(x, y, z, t) = -z \frac{\partial W}{\partial y} \\ w(x, y, z, t) = W(x, y, t) \end{cases} \quad (1)$$

where u, v, w are the displacements of point M in the x, y, z -directions, and
 U, V, W are the displacements of the projection P of point M on the middle
 surface of the plate. β_y and β_x are the rotations of the middle plane about the
 125 x and y axes, respectively, expressed as equations:

$$\begin{cases} \beta_x = -\frac{\partial W}{\partial x} \\ \beta_y = \frac{\partial W}{\partial y} \end{cases} \quad (2)$$

1
2
3
4
5
6
7
8
9
10
11
12
13
14
15
16
17
18
19
20
21
22
23
24
25
26
27
28
29
30
31
32
33
34
35
36
37
38
39
40
41
42
43
44
45
46
47
48
49
50
51
52
53
54
55
56
57
58
59
60
61
62
63
64
65

2.2. Constitutive equations

For plates with orientation such that orthotropic axes 1 and 2 are equal to the x and y axes, respectively, the force/displacement relationships are expressed as equations:

$$\begin{cases} M_x = -\frac{h^3}{12}D_{11}\frac{\partial^2 w}{\partial x^2} - \frac{h^3}{12}D_{12}\frac{\partial^2 w}{\partial y^2} \\ M_y = -\frac{h^3}{12}D_{12}\frac{\partial^2 w}{\partial x^2} - \frac{h^3}{12}D_{22}\frac{\partial^2 w}{\partial y^2} \\ M_{xy} = -\frac{h^3}{6}D_{66}\frac{\partial^2 w}{\partial x\partial y} \end{cases} \quad (3)$$

130

$$\begin{cases} T_x = -\frac{h^3}{12}D_{11}\frac{\partial^3 w}{\partial x^3} - \frac{h^3}{12}(D_{12} + 2D_{66})\frac{\partial^3 w}{\partial x\partial y^2} \\ T_y = -\frac{h^3}{12}D_{22}\frac{\partial^3 w}{\partial y^3} - \frac{h^3}{12}(D_{12} + 2D_{66})\frac{\partial^3 w}{\partial x^2\partial y} \end{cases} \quad (4)$$

where

$$\begin{cases} D_{11} = \frac{E_1}{1-\nu_{12}\nu_{21}} \\ D_{22} = \frac{E_2}{1-\nu_{12}\nu_{21}} \\ D_{12} = \frac{\nu_{12}E_2}{1-\nu_{12}\nu_{21}} \\ D_{66} = G_{12} \end{cases} \quad (5)$$

where E_1, E_2 are the Young's moduli along the orthotropic directions, ν_{12} and ν_{21} are Poisson's ratios, and G_{12} is the shear modulus.

135

1
2
3
4
5
6
7
8
9
10
11
12
13
14
15
16
17
18
19
20
21
22
23
24
25
26
27
28
29
30
31
32
33
34
35
36
37
38
39
40
41
42
43
44
45
46
47
48
49
50
51
52
53
54
55
56
57
58
59
60
61
62
63
64
65

2.3. *Boundary conditions*

Natural boundary conditions along the boundaries $x = \pm a$ are easily written using the Hamilton's principle; they can be expressed as equations:

$$\begin{cases} T_x + \frac{\partial M_{xy}}{\partial y} = \mathcal{F}_{zx} \\ M_x = \mathcal{M}_x \end{cases} \quad (6)$$

Similarly, the natural boundary conditions along $y = \pm b$ can be expressed as equations:

$$\begin{cases} T_y + \frac{\partial M_{xy}}{\partial x} = \mathcal{F}_{zy} \\ M_y = \mathcal{M}_y \end{cases} \quad (7)$$

2.4. *Equation of motion*

Equilibrium relationships are expressed as equation:

$$\frac{\partial^2 M_x}{\partial x^2} + 2 \frac{\partial^2 M_{xy}}{\partial x \partial y} + \frac{\partial^2 M_y}{\partial y^2} = \rho h \frac{\partial^2 w}{\partial t^2} \quad (8)$$

The equation of motion of a thin plate is obtained by introducing force/displacement relationships into the equilibrium equations, expressed as equation:

$$-\frac{h^3}{12} D_{11} \frac{\partial^4 w}{\partial x^4} - \left(\frac{h^3}{6} D_{12} + \frac{h^3}{3} D_{66} \right) \frac{\partial^4 w}{\partial x^2 \partial y^2} - \frac{h^3}{12} D_{22} \frac{\partial^4 w}{\partial y^4} = \rho h \frac{\partial^2 w}{\partial t^2} \quad (9)$$

1
2
3
4
5
6
7
8
9
10
11
12
13
14
15
16
17
18
19
20
21
22
23
24
25
26
27
28
29
30
31
32
33
34
35
36
37
38
39
40
41
42
43
44
45
46
47
48
49
50
51
52
53
54
55
56
57
58
59
60
61
62
63
64
65

145 **3. New Lévy series solution**

For harmonic vibrations, the transverse displacement can be expressed as follows:

$$w(x, y, t) = W(x, y)e^{i\omega t} \quad (10)$$

and the amplitude of the harmonic solution satisfies the following:

$$-\frac{h^3}{12}D_{11}\frac{\partial^4 W}{\partial x^4} - \left(\frac{h^3}{6}D_{12} + \frac{h^3}{3}D_{66}\right)\frac{\partial^4 W}{\partial x^2\partial y^2} - \frac{h^3}{12}D_{22}\frac{\partial^4 W}{\partial y^4} + \rho h\omega^2 W = 0 \quad (11)$$

The Gorman superposition method facilitates the analysis of only one quarter
150 of the rectangular plate for each symmetry contribution; the novel Lévy series
simplifies the problem, providing a general exact solution of the governing equa-
tion without dividing the displacement into four symmetry contributions. The
proposed Lévy series can be expressed as follows:

$$W(x, y) = \sum_{m=0}^{+\infty} {}_1W_m(x) \cos \frac{m\pi y}{b} + \sum_{m=0}^{+\infty} {}_2W_m(y) \cos \frac{m\pi x}{a} \quad (12)$$

$$+ \sum_{m=1}^{+\infty} {}_3W_m(x) \sin \frac{(2m-1)\pi y}{2b} + \sum_{m=1}^{+\infty} {}_4W_m(y) \sin \frac{(2m-1)\pi x}{2a}$$

Therefore, the rotations β_x, β_y defined by Eqs. 2 are expressed as follows:

$$\left\{ \begin{array}{l} \beta_x(x, y) = -\sum_{m=0}^{+\infty} {}_1W'_m(x) \cos \frac{m\pi y}{b} + \sum_{m=0}^{+\infty} \frac{m\pi}{a} {}_2W_m(y) \sin \frac{m\pi x}{a} \\ \quad - \sum_{m=1}^{+\infty} {}_3W'_m(x) \sin \frac{(2m-1)\pi y}{2b} - \sum_{m=1}^{+\infty} \frac{(2m-1)\pi}{2a} {}_4W_m(y) \cos \frac{(2m-1)\pi x}{2a} \\ \beta_y(x, y) = -\sum_{m=0}^{+\infty} \frac{m\pi}{b} {}_1W_m(x) \sin \frac{m\pi y}{b} + \sum_{m=0}^{+\infty} {}_2W'_m(y) \cos \frac{m\pi x}{a} \\ \quad + \sum_{m=1}^{+\infty} \frac{(2m-1)\pi}{2b} {}_3W_m(x) \cos \frac{(2m-1)\pi y}{2b} + \sum_{m=1}^{+\infty} {}_4W'_m(y) \sin \frac{(2m-1)\pi x}{2a} \end{array} \right. \quad (13)$$

1
2
3
4
5
6
7
8
9
10
11
12
13
14
15
16
17
18
19
20
21
22
23
24
25
26
27
28
29
30
31
32
33
34
35
36
37
38
39
40
41
42
43
44
45
46
47
48
49
50
51
52
53
54
55
56
57
58
59
60
61
62
63
64
65

155 The idea is to avoid the Gorman superposition, which requires uncoupled sym-
metry contributions. This uncoupling hypothesis is valid solely when the ge-
ometry and materials have the same symmetry properties. This is not the case
when the orthotropic directions are not parallel to the edges of the plate or
when the plate is a parallelogram. Let us consider a nontrivial solution for
160 the harmonic equation of motion Eq. 11 denoted by W . Symmetric-symmetric,
antisymmetric-symmetric, symmetric-antisymmetric, and antisymmetric-antisymmetric
contributions are given below:

$$\left\{ \begin{array}{l} W_{SS}(x, y) = \frac{1}{4} [W(x, y) + W(-x, y) + W(x, -y) + W(-x, -y)] = W_{SS}(-x, y) = W_{SS}(x, -y) \\ W_{SA}(x, y) = \frac{1}{4} [W(x, y) + W(-x, y) - W(x, -y) - W(-x, -y)] = W_{SA}(-x, y) = -W_{SA}(x, -y) \\ W_{AS}(x, y) = \frac{1}{4} [W(x, y) - W(-x, y) + W(x, -y) - W(-x, -y)] = -W_{AS}(-x, y) = W_{AS}(x, -y) \\ W_{AA}(x, y) = \frac{1}{4} [W(x, y) - W(-x, y) - W(x, -y) + W(-x, -y)] = -W_{AA}(-x, y) = -W_{AA}(x, -y) \end{array} \right. \quad (14)$$

These contributions are such that $W(x, y) = W_{SS}(x, y) + W_{SA}(x, y) + W_{AS}(x, y) + W_{AA}(x, y)$, each of which satisfies the equation of harmonic motion, i.e., Eq. 11.

165 This property is the basis of Gorman decomposition. In this case, the symmetry contributions are uncoupled. For example, the symmetric-symmetric contribution is as follows:

$$\begin{aligned} \frac{\partial^4 W_{SS}}{\partial x^4} &= \frac{1}{4} \left[\frac{\partial^4 W}{\partial x^4}(x, y) + \frac{\partial^4 W}{\partial x^4}(-x, y) + \frac{\partial^4 W}{\partial x^4}(x, -y) + \frac{\partial^4 W}{\partial x^4}(-x, -y) \right] \\ \frac{\partial^4 W_{SS}}{\partial x^2 \partial y^2} &= \frac{1}{4} \left[\frac{\partial^4 W}{\partial x^2 \partial y^2}(x, y) + \frac{\partial^4 W}{\partial x^2 \partial y^2}(-x, y) + \frac{\partial^4 W}{\partial x^2 \partial y^2}(x, -y) + \frac{\partial^4 W}{\partial x^2 \partial y^2}(-x, -y) \right] \\ \frac{\partial^4 W_{SS}}{\partial y^4} &= \frac{1}{4} \left[\frac{\partial^4 W}{\partial y^4}(x, y) + \frac{\partial^4 W}{\partial y^4}(-x, y) + \frac{\partial^4 W}{\partial y^4}(x, -y) + \frac{\partial^4 W}{\partial y^4}(-x, -y) \right] \end{aligned} \quad (15)$$

1
2
3
4
5
6
7
8
9
10
11
12
13
14
15
16
17
18
19
20
21
22
23
24
25
26
27
28
29
30
31
32
33
34
35
36
37
38
39
40
41
42
43
44
45
46
47
48
49
50
51
52
53
54
55
56
57
58
59
60
61
62
63
64
65

Further, the following can be easily verified:

$$\alpha \frac{\partial^4 W_{SS}}{\partial x^4} + \beta \frac{\partial^4 W_{SS}}{\partial x^2 \partial y^2} + \gamma \frac{\partial^4 W_{SS}}{\partial y^4} = 0 \quad (16)$$

¹⁷⁰ α, β, γ being any real numbers.

Let us now consider a harmonic equation of motion that is slightly more complicated, such as

$$\alpha \frac{\partial^4 W}{\partial x^4} + \beta \frac{\partial^4 W}{\partial x \partial y^3} + \gamma \frac{\partial^4 W}{\partial y^4} + \delta W = 0 \quad (17)$$

$\alpha, \beta, \gamma, \delta$ being any real numbers.

¹⁷⁵

For example, the symmetric-symmetric contribution satisfies the following:

$$\frac{\partial^4 W_{SS}}{\partial x \partial y^3} = \frac{1}{4} \left[\frac{\partial^4 W}{\partial x \partial y^3}(x, y) - \frac{\partial^4 W}{\partial x \partial y^3}(-x, y) - \frac{\partial^4 W}{\partial x \partial y^3}(x, -y) + \frac{\partial^4 W}{\partial x \partial y^3}(-x, -y) \right] \quad (18)$$

Further, it can be easily verified that this contribution does not satisfy the modified harmonic equation of motion, i.e., Eq. 17. In this case, the symmetry contributions are coupled, and the Gorman decomposition does not apply.

¹⁸⁰

Without the use of the Gorman superposition and symmetry considerations, the proposed series provides novel perspectives for future DSM developments in which symmetry contributions are coupled. For uncoupled symmetry contri-

1
2
3
4
5
6
7
8
9
10
11
12
13
14
15
16
17
18
19
20
21
22
23
24
25
26
27
28
29
30
31
32
33
34
35
36
37
38
39
40
41
42
43
44
45
46
47
48
49
50
51
52
53
54
55
56
57
58
59
60
61
62
63
64
65

butions, these series facilitate the simplification of the dynamic stiffness matrix building procedure and the reduction of the total number of series. Here, four series are used where the Gorman superposition requires two series for each symmetry contribution, i.e., a total of eight series. Therefore, only the four family functions ${}_1W_m(x)$, ${}_2W_m(y)$, ${}_3W_m(x)$ and ${}_4W_m(y)$ have to be obtained. The procedure is described below.

First, the governing equations have to be solved under natural boundary conditions. Therefore, the Levy serie Eq. 12 are introduced into the equation of motion Eq. 11. Two uncoupled systems of differential equations along the x-axis and y-axis are obtained. These systems are given by equations:

$$\begin{cases} a_1 \frac{d^4 {}_1W_m}{dx^4} + a_2(m) \frac{d^2 {}_1W_m}{dx^2} + a_3(m) {}_1W_m = 0 \\ a'_1 \frac{d^4 {}_3W_m}{dx^4} + a'_2(m) \frac{d^2 {}_3W_m}{dx^2} + a'_3(m) {}_3W_m = 0 \end{cases} \quad (19)$$

$$\begin{cases} b_1 \frac{d^4 {}_2W_m}{dy^4} + b_2(m) \frac{d^2 {}_2W_m}{dy^2} + b_3(m) {}_2W_m = 0 \\ b'_1 \frac{d^4 {}_4W_m}{dy^4} + b'_2(m) \frac{d^2 {}_4W_m}{dy^2} + b'_3(m) {}_4W_m = 0 \end{cases} \quad (20)$$

where the coefficients a_i , a'_i , b_i and b'_i are expressed as

$$a_1 = -\frac{h^3}{12} D_{11}, \quad a_2(m) = \frac{h^3}{6} (D_{12} + 2D_{66}) \left(\frac{m\pi}{b}\right)^2, \quad a_3(m) = \left[\rho h \omega^2 - \frac{h^3}{12} D_{22} \left(\frac{m\pi}{b}\right)^4\right].$$

$$a'_1 = -\frac{h^3}{12} D_{11}, \quad a'_2(m) = \frac{h^3}{6} (D_{12} + 2D_{66}) \left(\frac{(2m-1)\pi}{2b}\right)^2, \quad a'_3(m) = \left[\rho h \omega^2 - \frac{h^3}{12} D_{22} \left(\frac{(2m-1)\pi}{2b}\right)^4\right].$$

1
2
3
4
5
6
7
8
9
10
11
12
13
14
15
16
17
18
19
20
21
22
23
24
25
26
27
28
29
30
31
32
33
34
35
36
37
38
39
40
41
42
43
44
45
46
47
48
49
50
51
52
53
54
55
56
57
58
59
60
61
62
63
64
65

$$b_1 = -\frac{\hbar^3}{12}D_{22}, \quad b_2(m) = \frac{\hbar^3}{6}(D_{12} + 2D_{66})\left(\frac{m\pi}{a}\right)^2, \quad b_3(m) = \left[\rho h \omega^2 - \frac{\hbar^3}{12}D_{11}\left(\frac{m\pi}{a}\right)^4\right]$$

$$b'_1 = -\frac{\hbar^3}{12}D_{22}, \quad b'_2(m) = \frac{\hbar^3}{6}(D_{12} + 2D_{66})\left(\frac{(2m-1)\pi}{2a}\right)^2, \quad b'_3(m) = \left[\rho h \omega^2 - \frac{\hbar^3}{12}D_{11}\left(\frac{(2m-1)\pi}{2a}\right)^4\right]$$

These systems of ordinary differential equations along the x-axis and y-axis are expressed as

$$\begin{cases} {}_1W_m''''(x) &= -\frac{a_2(m)}{a_1}{}_1W_m''(x) - \frac{a_3(m)}{a_1}{}_1W_m(x) \\ {}_3W_m''''(x) &= -\frac{a'_2(m)}{a'_1}{}_3W_m''(x) - \frac{a'_3(m)}{a'_1}{}_3W_m(x) \end{cases} \quad (21)$$

200

$$\begin{cases} {}_2W_m''''(y) &= -\frac{b_2(m)}{b_1}{}_2W_m''(y) - \frac{b_3(m)}{b_1b}{}_2W_m(y) \\ {}_4W_m''''(y) &= -\frac{b'_2(m)}{b'_1}{}_4W_m''(y) - \frac{b'_3(m)}{b'_1}{}_4W_m(y) \end{cases} \quad (22)$$

Applying the concept of state space, the two systems in Eqs. 21 and 22 can be transformed into matricial equations, respectively:

$${}_1Z'_m(x) = {}_1T_m {}_1Z_m(x), \quad {}_3Z'_m(x) = {}_3T_m {}_3Z_m(x) \quad (23)$$

$${}_2Z'_m(y) = {}_2T_m {}_2Z_m(y), \quad {}_4Z'_m(y) = {}_4T_m {}_4Z_m(y) \quad (24)$$

where

$${}_jZ_m(x) = [{}_jW_m(x), {}_jW'_m(x), {}_jW''_m(x), {}_jW'''_m(x)]^T, \quad j = 1, 3 \quad (25)$$

205 and

$${}_jZ_m(y) = [{}_jW_m(y), {}_jW'_m(y), {}_jW''_m(y), {}_jW'''_m(y)]^T, \quad j = 2, 4 \quad (26)$$

1
2
3
4
5
6
7
8
9
10
11
12
13
14
15
16
17
18
19
20
21
22
23
24
25
26
27
28
29
30
31
32
33
34
35
36
37
38
39
40
41
42
43
44
45
46
47
48
49
50
51
52
53
54
55
56
57
58
59
60
61
62
63
64
65

where

$${}^1T_m = \begin{pmatrix} 0 & 1 & 0 & 0 \\ 0 & 0 & 1 & 0 \\ 0 & 0 & 0 & 1 \\ -\frac{a_3(m)}{a_1} & 0 & -\frac{a_2(m)}{a_1} & 0 \end{pmatrix} \quad (27)$$

and

$${}^3T_m = \begin{pmatrix} 0 & 1 & 0 & 0 \\ 0 & 0 & 1 & 0 \\ 0 & 0 & 0 & 1 \\ -\frac{a'_3(m)}{a'_1} & 0 & -\frac{a'_2(m)}{a'_1} & 0 \end{pmatrix} \quad (28)$$

$${}^2T_m = \begin{pmatrix} 0 & 1 & 0 & 0 \\ 0 & 0 & 1 & 0 \\ 0 & 0 & 0 & 1 \\ -\frac{b_3(m)}{b_1} & 0 & -\frac{b_2(m)}{b_1} & 0 \end{pmatrix} \quad (29)$$

and

$${}^4T_m = \begin{pmatrix} 0 & 1 & 0 & 0 \\ 0 & 0 & 1 & 0 \\ 0 & 0 & 0 & 1 \\ -\frac{b'_3(m)}{b'_1} & 0 & -\frac{b'_2(m)}{b'_1} & 0 \end{pmatrix} \quad (30)$$

²¹⁰ The general solutions of Eqs. 23 and 24 are readily found using the distinct eigenvalues and corresponding matrix of eigenvectors of the companion matrices

1
2
3
4
5
6
7
8
9
10
11
12
13
14
15
16
17
18
19
20
21
22
23
24
25
26
27
28
29
30
31
32
33
34
35
36
37
38
39
40
41
42
43
44
45
46
47
48
49
50
51
52
53
54
55
56
57
58
59
60
61
62
63
64
65

${}^1T_m, {}^2T_m, {}^3T_m$ and 4T_m . These solutions are expressed as

$$\begin{cases} {}^1Z_m(x) = \sum_{i=1}^4 {}^iA_m {}^i\mathbf{Q}_m e^{i\lambda_m x} \\ {}^3Z_m(x) = \sum_{i=5}^8 {}^iA_m {}^i\mathbf{Q}_m e^{i\lambda_m x} \\ {}^2Z_m(y) = \sum_{i=9}^{12} {}^iA_m {}^i\mathbf{Q}_m e^{i\lambda_m y} \\ {}^4Z_m(y) = \sum_{i=13}^{16} {}^iA_m {}^i\mathbf{Q}_m e^{i\lambda_m y} \end{cases} \quad (31)$$

where ${}^i\mathbf{Q}_m$ and ${}^i\lambda_m$ are the eigenvectors and the eigenvalues, respectively, of the matrices iT_m for $i \in \{1, 2, 3, 4\}$, ${}^i\mathbf{Q}_m$ and ${}^i\lambda_m$ are the eigenvectors and the eigenvalues of the matrices 3T_m for $i \in \{5, 6, 7, 8\}$.

Similarly, ${}^i\mathbf{Q}_m$ and ${}^i\lambda_m$ are the eigenvectors and the eigenvalues, respectively, of the matrices 2T_m for $i \in \{9, 10, 11, 13\}$; ${}^i\mathbf{Q}_m$ and ${}^i\lambda_m$ are the eigenvectors and eigenvalues, respectively, of the matrices 4T_m for $i \in \{13, 14, 15, 16\}$.

220

The functions ${}_1W_m, {}_3W_m$ along the x -direction and ${}_2W_m, {}_4W_m$ along the y -direction can be expanded as

1
2
3
4
5
6
7
8
9
10
11
12
13
14
15
16
17
18
19
20
21
22
23
24
25
26
27
28
29
30
31
32
33
34
35
36
37
38
39
40
41
42
43
44
45
46
47
48
49
50
51
52
53
54
55
56
57
58
59
60
61
62
63
64
65

$$\left\{ \begin{array}{l} {}_1W_m(x) = \sum_{i=1}^4 {}^iA_m {}^1Q_m e^{i\lambda_m x} \\ {}_1W'_m(x) = \sum_{i=1}^4 {}^iA_m {}^2Q_m e^{i\lambda_m x} \\ {}_1W''_m(x) = \sum_{i=1}^4 {}^iA_m {}^3Q_m e^{i\lambda_m x} \\ {}_1W'''_m(x) = \sum_{i=1}^4 {}^iA_m {}^4Q_m e^{i\lambda_m x} \\ {}_3W_m(x) = \sum_{i=5}^8 {}^iA_m {}^1Q_m e^{i\lambda_m x} \\ {}_3W'_m(x) = \sum_{i=5}^8 {}^iA_m {}^2Q_m e^{i\lambda_m x} \\ {}_3W''_m(x) = \sum_{i=5}^8 {}^iA_m {}^3Q_m e^{i\lambda_m x} \\ {}_3W'''_m(x) = \sum_{i=5}^8 {}^iA_m {}^4Q_m e^{i\lambda_m x} \end{array} \right. \quad (32)$$

where ${}^1Q_m, {}^2Q_m, {}^3Q_m, {}^4Q_m$ are the components of vector ${}^i\mathbf{Q}_m$ with $i \in$
 $\{1, \dots, 8\}$ and

$$\left\{ \begin{array}{l} {}_2W_m(y) = \sum_{i=9}^{12} {}^iA_m {}^1Q_m e^{i\lambda_m y} \\ {}_2W'_m(y) = \sum_{i=9}^{12} {}^iA_m {}^2Q_m e^{i\lambda_m y} \\ {}_2W''_m(y) = \sum_{i=9}^{12} {}^iA_m {}^3Q_m e^{i\lambda_m y} \\ {}_2W'''_m(y) = \sum_{i=9}^{12} {}^iA_m {}^4Q_m e^{i\lambda_m y} \\ {}_4W_m(y) = \sum_{i=13}^{16} {}^iA_m {}^1Q_m e^{i\lambda_m y} \\ {}_4W'_m(y) = \sum_{i=13}^{16} {}^iA_m {}^2Q_m e^{i\lambda_m y} \\ {}_4W''_m(y) = \sum_{i=13}^{16} {}^iA_m {}^3Q_m e^{i\lambda_m y} \\ {}_4W'''_m(y) = \sum_{i=13}^{16} {}^iA_m {}^4Q_m e^{i\lambda_m y} \end{array} \right. \quad (33)$$

where ${}^1Q_m, {}^2Q_m, {}^3Q_m, {}^4Q_m$ are the components of vector ${}^i\mathbf{Q}_m$ with $i \in$
 $\{9, \dots, 16\}$.

For $m = 0$, a simpler expression of the solution is possible. The functions

1
2
3
4
5
6
7
8
9
10
11
12
13
14
15
16
17
18
19
20
21
22
23
24
25
26
27
28
29
30
31
32
33
34
35
36
37
38
39
40
41
42
43
44
45
46
47
48
49
50
51
52
53
54
55
56
57
58
59
60
61
62
63
64
65

²³⁰ ${}_1W_0(x)$ and ${}_2W_0(y)$ are the solutions, expressed as equations:

$$\begin{cases} -\frac{h^3}{12}Q_{11}\frac{d^4{}_1W_0}{dx^4} = -\rho h\omega^2{}_1W_0(x) \\ -\frac{h^3}{12}Q_{22}\frac{d^4{}_2W_0}{dy^4} = -\rho h\omega^2{}_2W_0(y) \end{cases} \quad (34)$$

therefore,

$$\begin{cases} {}_1W_0(x) = \sum_{i=1}^4 {}^iA_0e^{i\lambda_0x} \\ {}_2W_0(y) = \sum_{i=5}^8 {}^iA_0e^{i\lambda_0y} \end{cases} \quad (35)$$

where eigenvalues ${}^i\lambda_0$ are expressed as

$$\begin{cases} {}^1\lambda_0 = \sqrt[4]{\frac{12\rho w^2}{Q_{11}h^2}} & {}^5\lambda_0 = \sqrt[4]{\frac{12\rho w^2}{Q_{22}h^2}} \\ {}^2\lambda_0 = -\sqrt[4]{\frac{12\rho w^2}{Q_{11}h^2}} & {}^6\lambda_0 = -\sqrt[4]{\frac{12\rho w^2}{Q_{22}h^2}} \\ {}^3\lambda_0 = i\sqrt[4]{\frac{12\rho w^2}{Q_{11}h^2}} & {}^7\lambda_0 = i\sqrt[4]{\frac{12\rho w^2}{Q_{22}h^2}} \\ {}^4\lambda_0 = -i\sqrt[4]{\frac{12\rho w^2}{Q_{11}h^2}} & {}^8\lambda_0 = -i\sqrt[4]{\frac{12\rho w^2}{Q_{22}h^2}} \end{cases} \quad (36)$$

The transverse displacement $W(x, y)$ is obtained from Eqs. 32, 33 and 12, expressed as

$$\begin{aligned} W(x, y) &= \sum_{i=1}^4 {}^iA_0e^{i\lambda_0x} + \sum_{i=5}^8 {}^iA_0e^{i\lambda_0y} \\ &+ \sum_{m=1}^{+\infty} \sum_{i=1}^4 {}^iA_m {}^{1i}Q_m e^{i\lambda_m x} \cos \frac{m\pi y}{b} + \sum_{m=1}^{+\infty} \sum_{i=9}^{12} {}^iA_m {}^{1i}Q_m e^{i\lambda_m y} \cos \frac{m\pi x}{a} \\ &+ \sum_{m=1}^{+\infty} \sum_{i=5}^8 {}^iA_m {}^{1i}Q_m e^{i\lambda_m x} \sin \frac{(2m-1)\pi y}{2b} + \sum_{m=1}^{+\infty} \sum_{i=13}^{16} {}^iA_m {}^{1i}Q_m e^{i\lambda_m y} \sin \frac{(2m-1)\pi x}{2a} \end{aligned} \quad (37)$$

At this stage, the four family functions ${}_1W_m(x)$, ${}_2W_m(y)$, ${}_3W_m(x)$ and ${}_4W_m(y)$ are processed, and the displacement solution in the whole plate is known.

1
2
3
4
5
6
7
8
9
10
11
12
13
14
15
16
17
18
19
20
21
22
23
24
25
26
27
28
29
30
31
32
33
34
35
36
37
38
39
40
41
42
43
44
45
46
47
48
49
50
51
52
53
54
55
56
57
58
59
60
61
62
63
64
65

The rotations are obtained from Eqs. 32, 33 and 13 in the following form:

$$\begin{aligned}
\beta_x(x, y) &= -\sum_{i=1}^4 {}^i A_0 {}^i \lambda_0 e^{i \lambda_0 x} - \sum_{m=1}^{+\infty} \sum_{i=1}^4 {}^i A_m {}^{2i} Q_m e^{i \lambda_m x} \cos \frac{m \pi y}{b} \\
&+ \sum_{m=1}^{+\infty} \sum_{i=9}^{12} {}^i A_m {}^{1i} Q_m e^{i \lambda_m y} \left(\frac{m \pi}{a} \right) \sin \frac{\pi x}{a} - \sum_{m=1}^{+\infty} \sum_{i=5}^8 {}^i A_m {}^{2i} Q_m e^{i \lambda_m x} \sin \frac{(2m-1) \pi y}{2b} \\
&- \sum_{m=1}^{+\infty} \sum_{i=13}^{16} {}^i A_m {}^{1i} Q_m e^{i \lambda_m y} \left(\frac{(2m-1) \pi}{2a} \right) \cos \frac{(2m-1) \pi x}{2a}
\end{aligned} \tag{38}$$

$$\begin{aligned}
\beta_y(x, y) &= \sum_{i=5}^8 {}^i A_0 {}^i \lambda_0 e^{i \lambda_0 y} - \sum_{m=1}^{+\infty} \sum_{i=1}^4 {}^i A_m {}^{1i} Q_m e^{i \lambda_m x} \left(\frac{m \pi}{b} \right) \sin \frac{m \pi y}{b} \\
&+ \sum_{m=1}^{+\infty} 2 \sum_{i=9}^{12} {}^i A_m {}^{2i} Q_m e^{i \lambda_m y} \cos \frac{m \pi x}{a} + \sum_{m=1}^{+\infty} \sum_{i=5}^8 {}^i A_m {}^{1i} Q_m e^{i \lambda_m x} \left(\frac{(2m-1) \pi}{2b} \right) \cos \frac{(2m-1) \pi y}{2b} \\
&+ \sum_{m=1}^{+\infty} \sum_{i=13}^{16} {}^i A_m {}^{2i} Q_m e^{i \lambda_m y} \sin \frac{(2m-1) \pi x}{2a}
\end{aligned} \tag{39}$$

4. Dynamic stiffness matrix of the completely free orthotropic plate

As explained in the Introduction, a solution under a fully natural boundary condition is required to allow the assembly of dynamic stiffness matrices. The dynamic stiffness matrices of the FFFF plate elements can be assembled as with the FEM. Therefore, the integration constants are eliminated in the FFFF case. This boundary condition is not a limitation for the other boundary condition cases. Similar to the FE stiffness and mass matrices, the FFFF dynamic stiffness matrix can be modified to consider a simply supported condition or a clamped condition with a penalty method or simply with line and column removals. The only case that was not included was the fully clamped plate. In this particular case, the assembly of two FFFF matrices and modification of the global matrix are required.

1
2
3
4
5
6
7
8
9
10
11
12
13
14
15
16
17
18
19
20
21
22
23
24
25
26
27
28
29
30
31
32
33
34
35
36
37
38
39
40
41
42
43
44
45
46
47
48
49
50
51
52
53
54
55
56
57
58
59
60
61
62
63
64
65

The displacement vector \tilde{u} of the boundaries $x = a$, $y = b$, $x = -a$ and $y = -b$ is defined as

$$\tilde{u} = \begin{pmatrix} w_0(a, y) \\ \beta_x(a, y) \\ w_0(x, b) \\ \beta_y(x, b) \\ w_0(-a, y) \\ \beta_x(-a, y) \\ w_0(x, -b) \\ \beta_y(x, -b) \end{pmatrix} \quad (40)$$

Using the natural boundary conditions in Eqs. 6 and 7, the external force vectors \tilde{f} on these boundaries are defined as

$$\tilde{f} = \begin{pmatrix} \mathcal{F}_{zx}(a, y) \\ \mathcal{M}_x(a, y) \\ \mathcal{F}_{zy}(x, b) \\ \mathcal{M}_y(x, b) \\ -\mathcal{F}_{zx}(-a, y) \\ -\mathcal{M}_x(-a, y) \\ -\mathcal{F}_{zy}(x, -b) \\ -\mathcal{M}_y(x, -b) \end{pmatrix} \quad (41)$$

Applying the projection method [19], the dependence of \tilde{u} and \tilde{f} with the spatial variables x and y is eliminated. The components of vectors \tilde{u} and \tilde{f} are

260 developed on a Hilbert basis series as

$$\tilde{u} = \begin{pmatrix} \frac{1}{S}W_0 + \sum_{n=1}^N \frac{1}{S}W_n \cos \frac{n\pi y}{b} + \sum_{n=1}^N \frac{1}{A}W_n \sin \frac{(2n-1)\pi y}{2b} \\ \frac{1}{S}\beta_{x0} + \sum_{n=1}^N \frac{1}{S}\beta_{xn} \cos \frac{n\pi y}{b} + \sum_{n=1}^N \frac{1}{A}\beta_{xn} \sin \frac{(2n-1)\pi y}{2b} \\ \frac{2}{S}W_0 + \sum_{n=1}^N \frac{2}{S}W_n \cos \frac{n\pi x}{a} + \sum_{n=1}^N \frac{2}{A}W_n \sin \frac{(2n-1)\pi x}{2a} \\ \frac{2}{S}\beta_{y0} + \sum_{n=1}^N \frac{2}{S}\beta_{yn} \cos \frac{n\pi x}{a} + \sum_{n=1}^N \frac{2}{A}\beta_{yn} \sin \frac{(2n-1)\pi x}{2a} \\ \frac{3}{S}W_0 + \sum_{n=1}^N \frac{3}{S}W_n \cos \frac{n\pi y}{b} + \sum_{n=1}^N \frac{3}{A}W_n \sin \frac{(2n-1)\pi y}{2b} \\ \frac{3}{S}\beta_{x0} + \sum_{n=1}^N \frac{3}{S}\beta_{xn} \cos \frac{n\pi y}{b} + \sum_{n=1}^N \frac{3}{A}\beta_{xn} \sin \frac{(2n-1)\pi y}{2b} \\ \frac{4}{S}W_0 + \sum_{n=1}^N \frac{4}{S}W_n \cos \frac{n\pi x}{a} + \sum_{n=1}^N \frac{4}{A}W_n \sin \frac{n\pi x}{a} \\ \frac{4}{S}\beta_{y0} + \sum_{n=1}^N \frac{4}{S}\beta_{yn} \cos \frac{n\pi x}{a} + \sum_{n=1}^N \frac{4}{A}\beta_{yn} \sin \frac{(2n-1)\pi x}{2a} \end{pmatrix} \quad (42)$$

$$\tilde{f} = \begin{pmatrix} \frac{1}{S}\mathcal{F}_{zx0} + \sum_{n=1}^N \frac{1}{S}\mathcal{F}_{zxn} \cos \frac{n\pi y}{b} + \sum_{n=1}^N \frac{1}{A}\mathcal{F}_{zxn} \sin \frac{(2n-1)\pi y}{2b} \\ \frac{1}{S}\mathcal{M}_{x0} + \sum_{n=1}^N \frac{1}{S}\mathcal{M}_{xn} \cos \frac{n\pi y}{b} + \sum_{n=1}^N \frac{1}{A}\mathcal{M}_{xn} \sin \frac{(2n-1)\pi y}{2b} \\ \frac{2}{S}\mathcal{F}_{zy0} + \sum_{n=1}^N \frac{2}{S}\mathcal{F}_{zyn} \cos \frac{n\pi x}{a} + \sum_{n=1}^N \frac{2}{A}\mathcal{F}_{zyn} \sin \frac{(2n-1)\pi x}{2a} \\ \frac{2}{S}\mathcal{M}_{y0} + \sum_{n=1}^N \frac{2}{S}\mathcal{M}_{yn} \cos \frac{n\pi x}{a} + \sum_{n=1}^N \frac{2}{A}\mathcal{M}_{yn} \sin \frac{(2n-1)\pi x}{2a} \\ -\frac{3}{S}\mathcal{F}_{zx0} - \sum_{n=1}^N \frac{3}{S}\mathcal{F}_{zxn} \cos \frac{n\pi y}{b} - \sum_{n=1}^N \frac{3}{A}\mathcal{F}_{zxn} \sin \frac{(2n-1)\pi y}{2b} \\ -\frac{3}{S}\mathcal{M}_{x0} - \sum_{n=1}^N \frac{3}{S}\mathcal{M}_{xn} \cos \frac{n\pi y}{b} - \sum_{n=1}^N \frac{3}{A}\mathcal{M}_{xn} \sin \frac{(2n-1)\pi y}{2b} \\ -\frac{4}{S}\mathcal{F}_{zy0} - \sum_{n=1}^N \frac{4}{S}\mathcal{F}_{zyn} \cos \frac{n\pi x}{a} - \sum_{n=1}^N \frac{4}{A}\mathcal{F}_{zyn} \sin \frac{(2n-1)\pi x}{2a} \\ -\frac{4}{S}\mathcal{M}_{y0} - \sum_{n=1}^N \frac{4}{S}\mathcal{M}_{yn} \cos \frac{n\pi x}{a} - \sum_{n=1}^N \frac{4}{A}\mathcal{M}_{yn} \sin \frac{(2n-1)\pi x}{2a} \end{pmatrix} \quad (43)$$

1
2
3
4
5
6
7
8
9
10
11
12
13
14
15
16
17
18
19
20
21
22
23
24
25
26
27
28
29
30
31
32
33
34
35
36
37
38
39
40
41
42
43
44
45
46
47
48
49
50
51
52
53
54
55
56
57
58
59
60
61
62
63
64
65

while

$$\begin{aligned}
 & \begin{bmatrix} {}^1_S W_0 \\ {}^1_S \beta_{x0} \\ {}^2_S W_0 \\ {}^2_S \beta_{x0} \\ {}^3_S W_0 \\ {}^3_S \beta_{y0} \\ {}^4_S W_0 \\ {}^4_S \beta_{y0} \end{bmatrix} = \begin{bmatrix} \frac{1}{2b} \int_{-b}^b W(a, y) dy \\ \frac{1}{2b} \int_{-b}^b \beta_x(a, y) dy \\ \frac{1}{2a} \int_{-a}^a W(x, b) dx \\ \frac{1}{2a} \int_{-a}^a \beta_y(x, b) dx \\ \frac{1}{2b} \int_{-b}^b W(-a, y) dy \\ \frac{1}{2b} \int_{-b}^b \beta_x(-a, y) dy \\ \frac{1}{2a} \int_{-a}^a W(x, -b) dx \\ \frac{1}{2a} \int_{-a}^a \beta_y(x, -b) dx \end{bmatrix} \quad \text{and} \quad \begin{bmatrix} {}^1_S W_n \\ {}^1_A W_n \\ {}^1_S \beta_{xn} \\ {}^1_A \beta_{xn} \\ {}^2_S W_n \\ {}^2_A W_n \\ {}^2_S \beta_{yn} \\ {}^2_A \beta_{yn} \\ {}^3_S W_n \\ {}^3_A W_n \\ {}^3_S \beta_{xn} \\ {}^3_A \beta_{xn} \\ {}^4_S W_n \\ {}^4_A W_n \\ {}^4_S \beta_{yn} \\ {}^4_A \beta_{yn} \end{bmatrix} = \begin{bmatrix} \frac{1}{b} \int_{-b}^b W(a, y) \cos \frac{n\pi y}{b} dy \\ \frac{1}{b} \int_{-b}^b W(a, y) \sin \frac{(2n-1)\pi y}{2b} dy \\ \frac{1}{b} \int_{-b}^b \beta_x(a, y) \cos \frac{n\pi y}{b} dy \\ \frac{1}{b} \int_{-b}^b \beta_x(a, y) \sin \frac{(2n-1)\pi y}{2b} dy \\ \frac{1}{a} \int_{-a}^a W(x, b) \cos \frac{n\pi x}{a} dx \\ \frac{1}{a} \int_{-a}^a W(x, b) \sin \frac{(2n-1)\pi x}{2a} dx \\ \frac{1}{a} \int_{-a}^a \beta_y(x, b) \cos \frac{n\pi x}{a} dx \\ \frac{1}{a} \int_{-a}^a \beta_y(x, b) \sin \frac{(2n-1)\pi x}{2a} dx \\ \frac{1}{b} \int_{-b}^b W(-a, y) \cos \frac{n\pi y}{b} dy \\ \frac{1}{b} \int_{-b}^b W(-a, y) \sin \frac{(2n-1)\pi y}{2b} dy \\ \frac{1}{b} \int_{-b}^b \beta_x(-a, y) \cos \frac{n\pi y}{b} dy \\ \frac{1}{b} \int_{-b}^b \beta_x(-a, y) \sin \frac{(2n-1)\pi y}{2b} dy \\ \frac{1}{a} \int_{-a}^a W(x, -b) \cos \frac{n\pi x}{a} dx \\ \frac{1}{a} \int_{-a}^a W(x, -b) \sin \frac{(2n-1)\pi x}{2a} dx \\ \frac{1}{a} \int_{-a}^a \beta_y(x, -b) \cos \frac{n\pi x}{a} dx \\ \frac{1}{a} \int_{-a}^a \beta_y(x, -b) \sin \frac{(2n-1)\pi x}{2a} dx \end{bmatrix} \quad (44)
 \end{aligned}$$

1
2
3
4
5
6
7
8
9
10
11
12
13
14
15
16
17
18
19
20
21
22
23
24
25
26
27
28
29
30
31
32
33
34
35
36
37
38
39
40
41
42
43
44
45
46
47
48
49
50
51
52
53
54
55
56
57
58
59
60
61
62
63
64
65

$$\begin{aligned}
& \begin{bmatrix} \frac{1}{S} \mathcal{F}_{zx0} \\ \frac{1}{S} \mathcal{M}_{x0} \\ \frac{2}{S} \mathcal{F}_{zy0} \\ \frac{2}{S} \mathcal{M}_{y0} \\ \frac{3}{S} \mathcal{F}_{zx0} \\ \frac{3}{S} \mathcal{M}_{x0} \\ \frac{4}{S} \mathcal{F}_{zy0} \\ \frac{4}{S} \mathcal{M}_{y0} \end{bmatrix} = \begin{bmatrix} \frac{1}{2b} \int_{-b}^b \mathcal{F}_{zx}(a, y) dy \\ \frac{1}{2b} \int_{-b}^b \mathcal{M}_x(a, y) dy \\ \frac{1}{2b} \int_{-a}^a \mathcal{F}_{zy}(x, b) dx \\ \frac{1}{2b} \int_{-a}^a \mathcal{M}_y(x, b) dx \\ \frac{1}{2a} \int_{-b}^b \mathcal{F}_{zx}(-a, y) dy \\ \frac{1}{2a} \int_{-b}^b \mathcal{M}_x(-a, y) dy \\ \frac{1}{2a} \int_{-a}^a \mathcal{F}_{zy}(x, -b) dx \\ \frac{1}{2a} \int_{-a}^a \mathcal{M}_y(x, -b) dx \end{bmatrix} \quad \text{and} \quad \begin{bmatrix} \frac{1}{S} \mathcal{F}_{zxn} \\ \frac{1}{A} \mathcal{F}_{zxn} \\ \frac{1}{S} \mathcal{M}_{xn} \\ \frac{1}{A} \mathcal{M}_{xn} \\ \frac{2}{S} \mathcal{F}_{zyn} \\ \frac{2}{A} \mathcal{F}_{zyn} \\ \frac{2}{S} \mathcal{M}_{yn} \\ \frac{2}{A} \mathcal{M}_{yn} \\ \frac{3}{S} \mathcal{F}_{zxn} \\ \frac{3}{A} \mathcal{F}_{zxn} \\ \frac{3}{S} \mathcal{M}_{xn} \\ \frac{3}{A} \mathcal{M}_{xn} \\ \frac{4}{S} \mathcal{F}_{zyn} \\ \frac{4}{A} \mathcal{F}_{zyn} \\ \frac{4}{S} \mathcal{M}_{yn} \\ \frac{4}{A} \mathcal{M}_{yn} \end{bmatrix} = \begin{bmatrix} \frac{1}{b} \int_{-b}^b \mathcal{F}_{zx}(a, y) \cos \frac{n\pi y}{b} dy \\ \frac{1}{b} \int_{-b}^b \mathcal{F}_{zx}(a, y) \sin \frac{(2n-1)\pi y}{2b} dy \\ \frac{1}{b} \int_{-b}^b \mathcal{M}_x(a, y) \cos \frac{n\pi y}{b} dy \\ \frac{1}{b} \int_{-b}^b \mathcal{M}_x(a, y) \sin \frac{(2n-1)\pi y}{2b} dy \\ \frac{1}{a} \int_{-a}^a \mathcal{F}_{zy}(x, b) \cos \frac{n\pi x}{a} dx \\ \frac{1}{a} \int_{-a}^a \mathcal{F}_{zy}(x, b) \sin \frac{(2n-1)\pi x}{2a} dx \\ \frac{1}{a} \int_{-a}^a \mathcal{M}_y(x, b) \cos \frac{n\pi x}{a} dx \\ \frac{1}{a} \int_{-a}^a \mathcal{M}_y(x, b) \sin \frac{(2n-1)\pi x}{2a} dx \\ \frac{1}{b} \int_{-b}^b \mathcal{F}_{zx}(-a, y) \cos \frac{n\pi y}{b} dy \\ \frac{1}{b} \int_{-b}^b \mathcal{F}_{zx}(-a, y) \sin \frac{(2n-1)\pi y}{2b} dy \\ \frac{1}{b} \int_{-b}^b \mathcal{M}_x(-a, y) \cos \frac{n\pi y}{b} dy \\ \frac{1}{b} \int_{-b}^b \mathcal{M}_x(-a, y) \sin \frac{(2n-1)\pi y}{2b} dy \\ \frac{1}{a} \int_{-a}^a \mathcal{F}_{zy}(x, b) \cos \frac{n\pi x}{a} dx \\ \frac{1}{a} \int_{-a}^a \mathcal{F}_{zy}(x, b) \sin \frac{(2n-1)\pi x}{2a} dx \\ \frac{1}{a} \int_{-a}^a \mathcal{M}_y(x, b) \cos \frac{n\pi x}{a} dx \\ \frac{1}{a} \int_{-a}^a \mathcal{M}_y(x, b) \sin \frac{(2n-1)\pi x}{2a} dx \end{bmatrix} \quad (45)
\end{aligned}$$

The subscripts x and y in Eqs. 42, 43, 44 and 45 refer to the plate boundaries
 $x = a$ or $x = -a$ and $y = -b$ or $y = b$. Instead of vectors \tilde{u} and \tilde{f} , projection
vectors \tilde{U} and \tilde{F} are derived. They are built with the components on the Hilbert
basis series expansion given by Eqs. 42 and 43. Thus, it is now possible to relate

1
2
3
4
5
6
7
8
9
10
11
12
13
14
15
16
17
18
19
20
21
22
23
24
25
26
27
28
29
30
31
32
33
34
35
36
37
38
39
40
41
42
43
44
45
46
47
48
49
50
51
52
53
54
55
56
57
58
59
60
61
62
63
64
65

displacement/force vectors and integration constants denoted as C_p :

$$\begin{aligned}\tilde{\mathbf{U}} &= \mathbf{H}(\omega)\mathbf{C}_p \\ \tilde{\mathbf{F}} &= \mathbf{G}(\omega)\mathbf{C}_p\end{aligned}\tag{46}$$

where

$$\begin{aligned}(\tilde{\mathbf{U}})^T &= [{}^1_S W_0 \quad {}^1_S \beta_{x0} \quad {}^2_S W_0 \quad {}^2_S \beta_{y0} \quad {}^3_S W_0 \quad {}^3_S \beta_{x0} \quad {}^4_S W_0 \quad {}^4_S \beta_{y0} \cdots \quad {}^1_S W_N \quad {}^1_A W_N \quad {}^1_S \beta_{xN} \quad {}^1_A \beta_{xN} \\ &\quad {}^2_S W_N \quad {}^2_A W_N \quad {}^1_S \beta_{yN} \quad {}^2_A \beta_{xN} \quad {}^3_S W_N \quad {}^3_A W_N \quad {}^3_S \beta_{xN} \quad {}^3_A \beta_{xN} \quad {}^4_S W_N \quad {}^4_A W_N \quad {}^4_S \beta_{yN} \quad {}^4_A \beta_{yN}]_{(8+16N)}\end{aligned}\tag{47}$$

$$\begin{aligned}(\tilde{\mathbf{F}})^T &= [{}^1_S \mathcal{F}_{zx0} \quad {}^1_S \mathcal{M}_{x0} \quad {}^2_S \mathcal{F}_{zy0} \quad {}^2_S \mathcal{M}_{y0} \quad {}^3_S \mathcal{F}_{zx0} \quad {}^3_S \mathcal{M}_{x0} \quad {}^4_S \mathcal{F}_{zy0} \quad {}^4_S \mathcal{M}_{y0} \cdots \quad {}^1_S \mathcal{F}_{zxN} \quad {}^1_A \mathcal{F}_{zxN} \quad {}^1_S \mathcal{M}_{xN} \\ &\quad {}^1_A \mathcal{M}_{xN} \quad {}^2_S \mathcal{F}_{zyN} \quad {}^2_A \mathcal{F}_{zyN} \quad {}^2_S \mathcal{M}_{yN} \quad {}^2_A \mathcal{M}_{yN} \quad {}^3_S \mathcal{F}_{zxN} \quad {}^3_A \mathcal{F}_{zxN} \quad {}^3_S \mathcal{M}_{xN} \quad {}^3_A \mathcal{M}_{xN} \quad {}^4_S \mathcal{F}_{zyN} \quad {}^4_A \mathcal{F}_{zyN} \\ &\quad {}^4_S \mathcal{M}_{yN} \quad {}^4_A \mathcal{M}_{yN}]_{(8+16N)}\end{aligned}\tag{48}$$

and

$$\begin{aligned}(\tilde{\mathbf{C}}_p)^T &= [{}^1 A_0 \quad {}^2 A_0 \quad {}^3 A_0 \quad {}^4 A_0 \quad {}^5 A_0 \quad {}^6 A_0 \quad {}^7 A_0 \quad {}^8 A_0 \cdots \quad {}^1 A_N \quad {}^2 A_N \quad {}^3 A_N \quad {}^4 A_N \\ &\quad {}^5 A_N \quad {}^6 A_N \quad {}^7 A_N \quad {}^8 A_N \quad {}^9 A_N \quad {}^{10} A_N \quad {}^{11} A_N \quad {}^{12} A_N \quad {}^{13} A_N \quad {}^{14} A_N \quad {}^{15} A_N \quad {}^{16} A_N]_{(8+16N)}\end{aligned}\tag{49}$$

The size of the matrices \mathbf{H} and \mathbf{G} depends on the number of terms in the general solution given by the Lévy series Eq. 12. To consider square matrices, the number of terms in the Lévy series must be the same as the number of terms in the Hilbert series expansion in Eqs. 42 and 43. Elimination of vector C_p from Eq. 46 gives the relation between the force vector $\tilde{\mathbf{F}}$ and the displacement

1
2
3
4
5
6
7
8
9
10
11
12
13
14
15
16
17
18
19
20
21
22
23
24
25
26
27
28
29
30
31
32
33
34
35
36
37
38
39
40
41
42
43
44
45
46
47
48
49
50
51
52
53
54
55
56
57
58
59
60
61
62
63
64
65

vector \tilde{U} , expressed as

$$\tilde{\mathbf{F}} = \mathbf{K} \cdot \tilde{\mathbf{U}} \tag{50}$$

where \mathbf{K} is the dynamic stiffness matrix for the entire plate. This matrix relates the projection vectors of displacements \tilde{U} and forces \tilde{F} on the four edges of the plate.

$$\mathbf{K}(\omega) = \mathbf{G}(\omega) \cdot \mathbf{H}(\omega)^{-1} \tag{51}$$

This building procedure leads to an $(8 + 16N) \times (8 + 16N)$ dynamic stiffness matrix. The dimensions of the matrix correspond to the selected Hilbert basis for the projections on each edge of the plate. Therefore, the proposed Lévy series does not exhibit an advantage over the previous Gorman decomposition procedure in terms of dimensions, as the projection Hilbert basis is identical for both. Only the CPU time for post-processing of the displacement inside the plate is reduced because four series are used instead of eight.

5. Numerical results and discussion

The formulation is based on the new Lévy series and has been implemented using FORTRAN and MATLAB programs. In this section, several numerical examples are discussed to establish the accuracy of the current formulation. Natural frequencies, mode shapes, and harmonic responses on an orthotropic plate with free boundary conditions were processed.

1
2
3
4
5
6
7
8
9
10
11
12
13
14
15
16
17
18
19
20
21
22
23
24
25
26
27
28
29
30
31
32
33
34
35
36
37
38
39
40
41
42
43
44
45
46
47
48
49
50
51
52
53
54
55
56
57
58
59
60
61
62
63
64
65

5.1. Modal analysis

295 The $2a \times 2b$ dimensions of the plate are 0.5 m \times 1 m, and its thickness is
0.002 m (Figure 1). The plate is constructed with a carbon-epoxy material; its
properties are $E_1=18.1$ GPa, $E_2=50.9$ GPa, $G_{12} = 11.0$ GPa, $\nu_{12} = 0.4$ and
 $\rho=1526$ kg/m³. The orthotropic directions are parallel to the edges of the plate.
Direction 1 is along the x direction and direction 2 is along the y direction. A
300 modal analysis was performed for FFFF boundary conditions. This calculation
provides a first validation of the developed element but is not sufficient because
the series are able to predict eigenfrequencies with high accuracy for very few
terms but necessitate much more terms to process harmonic responses over the
entire frequency range. This problem is illustrated in Figure 2. The harmonic
305 responses of the aforementioned plate were processed over [0,100 Hz] frequency
range while increasing the number of terms in the Lévy series. The convergence
of the response is clearly shown; however the convergence toward eigenfrequen-
cies is considerably easier than that of the response for other frequencies.

1
2
3
4
5
6
7
8
9
10
11
12
13
14
15
16
17
18
19
20
21
22
23
24
25
26
27
28
29
30
31
32
33
34
35
36
37
38
39
40
41
42
43
44
45
46
47
48
49
50
51
52
53
54
55
56
57
58
59
60
61
62
63
64
65

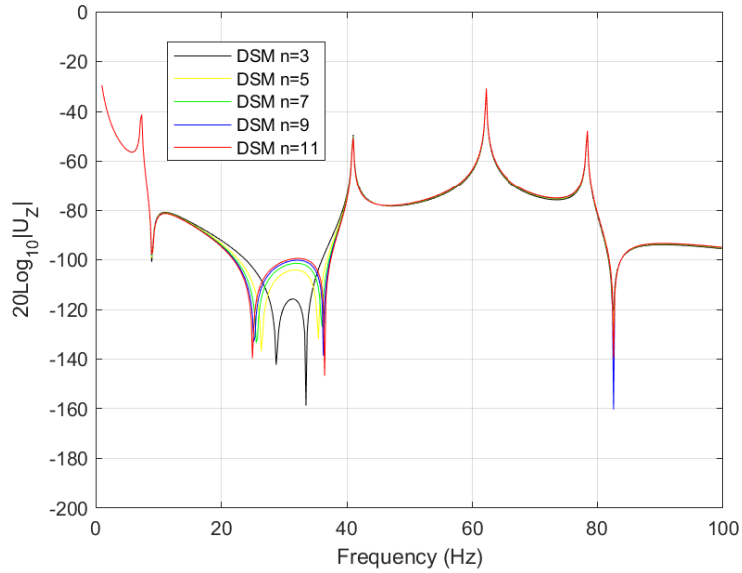


Figure 2: DSM convergence for SS harmonic response on [0, 100 Hz]

310 Eigenfrequencies are often obtained in DSM formulations using the William-
 Wittrick algorithm [40], [41], [15], [20]. In this study, these frequencies are simply
 evaluated using harmonic repetition analysis [19], [34]. Four load cases, exciting
 symmetric-symmetric (SS) modes, symmetric-antisymmetric (SA) modes
 (symmetric along x and antisymmetric along y), symmetric-antisymmetric (AS)
 315 modes (antisymmetric along x and symmetric along y) and antisymmetric-
 antisymmetric (AA) modes were considered. Peaks in displacement responses
 are detected. This method ensures that no eigenfrequencies are missing, especially
 when they are close together. Thus, modal displacements are obtained
 using the proposed Lévy series Eq. 12. The results are detailed for each load

1
2
3
4
5
6
7
8
9
10
11
12
13
14
15
16
17
18
19
20
21
22
23
24
25
26
27
28
29
30
31
32
33
34
35
36
37
38
39
40
41
42
43
44
45
46
47
48
49
50
51
52
53
54
55
56
57
58
59
60
61
62
63
64
65

320 case and compared with the FE modal analysis performed with the commercial software ABAQUS. Discrete Kirchhoff quadrilateral (DKQ) elements were used in the FE models. For the SS case, a convergence study of the DSM results is summarized in Table 1.

- 325 • Symmetric-symmetric modes.

Table 1: Natural frequencies of SS modes for orthotropic rectangular plate with FFFF boundary conditions for increasing n

SS Mode	1	2	3	4	5	6	7	8	9	10
DSM (n=3)	7.26	40.92	62.14	78.36	114.5	130.6	205.2		309.3	
DSM (n=5)	7.26	40.92	62.14	78.36	114.4	130.6	205.0	215.4	306.1	322.0
DSM (n=7)	7.26	40.92	62.14	78.36	114.4	130.6	205.0	215.4	306.0	321.9
DSM (n=9)	7.26	40.92	62.14	78.36	114.4	130.6	205.0	215.4	306.0	321.9
DSM (n=11)	7.26	40.92	62.14	78.36	114.4	130.6	205.0	215.4	306.0	321.9

Table 1 indicates that the first seven frequencies are exactly processed with only three terms, despite the fact that the harmonic response is very poor in this case (Figure 2). Moreover, we observed that some series have very good convergence toward eigenfrequencies that have been obtained with FE models; however, no convergence was obtained for any other frequency response.

Table 2 compares the FE and DSM results. The first ten eigenfrequencies corresponding to the symmetric-symmetric modes are given.

1
2
3
4
5
6
7
8
9
10
11
12
13
14
15
16
17
18
19
20
21
22
23
24
25
26
27
28
29
30
31
32
33
34
35
36
37
38
39
40
41
42
43
44
45
46
47
48
49
50
51
52
53
54
55
56
57
58
59
60
61
62
63
64
65

Table 2: Natural frequencies of SS modes for orthotropic rectangular plate with FFFF boundary conditions. DSM (n=11), DKQ FE (50×25, 67×33 and 100×50 elements)

SS Mode	1	2	3	4	5	6	7	8	9	10
DSM (n=11)	7.3	40.9	62.1	78.3	114.4	130.6	205.0	215.4	306	321.9
DKQ FE (100×50)	7.26	40.95	62.17	78.35	114.7	130.6	205.1	216.4	306.8	323.3
DKQ FE (67×33)	7.26	41.00	62.24	78.41	115.1	130.8	205.6	218.0	308.3	325.0
DKQ FE (50×25)	7.26	41.07	62.34	78.48	115.7	131.0	206.3	220.3	310.4	328.9

The convergence study of the FE results shows that more than 5000 DKQ finite elements are required to reach the precision of the DSM results.

- Symmetric-Antisymmetric modes.

Table 3 gives the first ten eigenfrequencies corresponding to the symmetric-antisymmetric modes.

Table 3: Natural frequencies of SA modes for orthotropic rectangular plate with FFFF boundary conditions. DSM (n=11), DKQ FE (100×50 elements)

SA Mode	1	2	3	4	5	6	7	8	9	10
DSM	24.1	63.1	125.8	167.3	186.9	228.3	245.1	324.2	359.3	437.7
DKQ FE	24.09	63.10	125.9	167.6	187.2	229.0	245.4	324.3	362.0	438.2

- Antisymmetric-Symmetric modes.

Table 4 gives the first ten eigenfrequencies corresponding to the antisymmetric-symmetric modes.

Table 4: Natural frequencies of AS modes for orthotropic rectangular plate with FFFF boundary conditions. DSM (n=11), DKQ FE (100×50 elements)

AS Mode	1	2	3	4	5	6	7	8	9	10
DSM	19.68	53.17	64.78	86.70	134.7	140.6	214.5	230.9	267.2	297.5
DKQ FE	19.67	53.16	64.77	86.65	134.7	140.6	214.3	230.8	267.1	297.3

1
2
3
4
5
6
7
8
9
10
11
12
13
14
15
16
17
18
19
20
21
22
23
24
25
26
27
28
29
30
31
32
33
34
35
36
37
38
39
40
41
42
43
44
45
46
47
48
49
50
51
52
53
54
55
56
57
58
59
60
61
62
63
64
65

- Antisymmetric-Antiymmetric modes.

Table 5 gives the first ten eigenfrequencies corresponding to the antisymmetric-antisymmetric modes.

Table 5: Natural frequencies of AA modes for orthotropic rectangular plate with FFFF boundary conditions. DSM (n=11), DKQ FE (100×50 elements)

AA Mode	1	2	3	4	5	6	7	8	9	10
DSM	11.00	37.97	81.45	137.8	158.3	171.3	228.3	254.3	308.0	377.6
DKQ FE	10.99	38.22	82.12	137.9	158.3	171.2	229.2	255.2	308.7	378.0

350

These tables show that the DSM formulation described in this study produces results in close agreement with FE results. Some representative mode shapes obtained by the DSM formulation are illustrated in Figure 3. Each mode shape is computed with the Lévy series Eq. 37 for a given eigenfrequency.

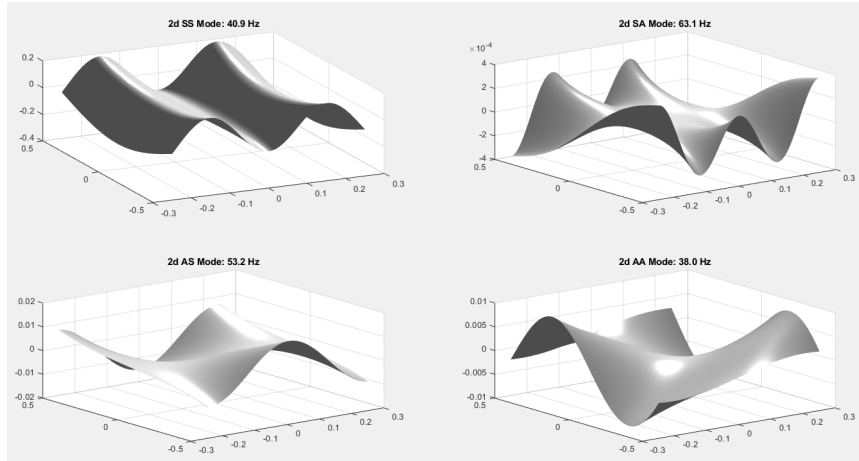


Figure 3: Second SS, AS, SA and AA mode shapes

1
2
3
4
5
6
7
8
9
10
11
12
13
14
15
16
17
18
19
20
21
22
23
24
25
26
27
28
29
30
31
32
33
34
35
36
37
38
39
40
41
42
43
44
45
46
47
48
49
50
51
52
53
54
55
56
57
58
59
60
61
62
63
64
65

355 As shown in Tables 2-5, the natural frequencies of the FFFF thin rectangular plate were calculated using the proposed DSM and were compared with the FEM results. Comparison of the natural frequencies shows that the average difference between DSM and FEM is practically negligible. In addition, using the proposed Lévy series, the mode shapes of thin rectangular plates can be 360 predicted, as presented in Figure 3. As explained above, such a modal analysis is not sufficient to validate the formulation. Harmonic responses are examined hereafter, and the numerical stability is estimated from the response curves for a given frequency range.

5.2. *Harmonic response analysis*

365 To evaluate the performance of the current formulation, several harmonic loadings were used, and the response of the plate was processed over the entire frequency range. The structure was subjected to harmonic forces distributed along the edges of the plate or located at a single point. Harmonic responses were evaluated for an increasing number of terms in series development (n=3, 370 n=7, and n=11). These responses were compared with those obtained using DKQ finite elements.

5.2.1. *Symmetrical-Symmetrical loading*

The structure was subjected to a unit harmonic force distributed along the 375 edges of the plate defined by $y = b$ and $y = -b$. The harmonic loading is shown in Figure 4.

1
2
3
4
5
6
7
8
9
10
11
12
13
14
15
16
17
18
19
20
21
22
23
24
25
26
27
28
29
30
31
32
33
34
35
36
37
38
39
40
41
42
43
44
45
46
47
48
49
50
51
52
53
54
55
56
57
58
59
60
61
62
63
64
65

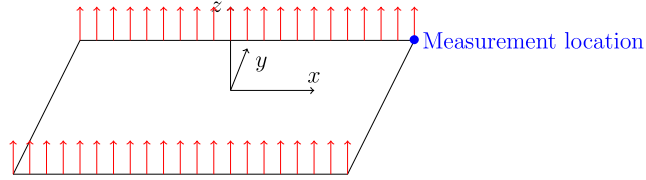


Figure 4: Symmetrical-symmetrical loading

The projections of this load on the functional basis must satisfy equations:

$$F_2(x) = {}_S^2 F_0 + \sum_{n=1}^N {}_S^2 F_n \cos \frac{n\pi x}{a} + \sum_{n=1}^N {}_A^2 F_n \sin \frac{(2n-1)\pi x}{2a} \quad (52)$$

and

$$F_4(x) = {}_S^4 F_0 + \sum_{n=1}^N {}_S^4 F_n \cos \frac{n\pi x}{a} + \sum_{n=1}^N {}_A^4 F_n \sin \frac{(2n-1)\pi x}{2a} \quad (53)$$

therefore, by identification, the following components on the Hilbert basis are

380 obtained: ${}_S^2 F_0 = 1$ and ${}_S^4 F_0 = 1$.

The harmonic response of the plate is evaluated at the point located at $x = a$ and $y = b$ on edge 1 according to the Hilbert basis in Eq. 42.

$$W(a, b) = {}_S^1 W_0 + \sum_{n=1}^N {}_S^1 W_n (-1)^n + \sum_{n=1}^N {}_A^1 W_n (-1)^{n+1} \quad (54)$$

The response obtained by DSM for $n=11$ terms in series and the response
385 obtained with 50×100 DKQ finite elements up to 500 Hz are shown in Figure
5. The two methods indicate very good agreement.

1
2
3
4
5
6
7
8
9
10
11
12
13
14
15
16
17
18
19
20
21
22
23
24
25
26
27
28
29
30
31
32
33
34
35
36
37
38
39
40
41
42
43
44
45
46
47
48
49
50
51
52
53
54
55
56
57
58
59
60
61
62
63
64
65

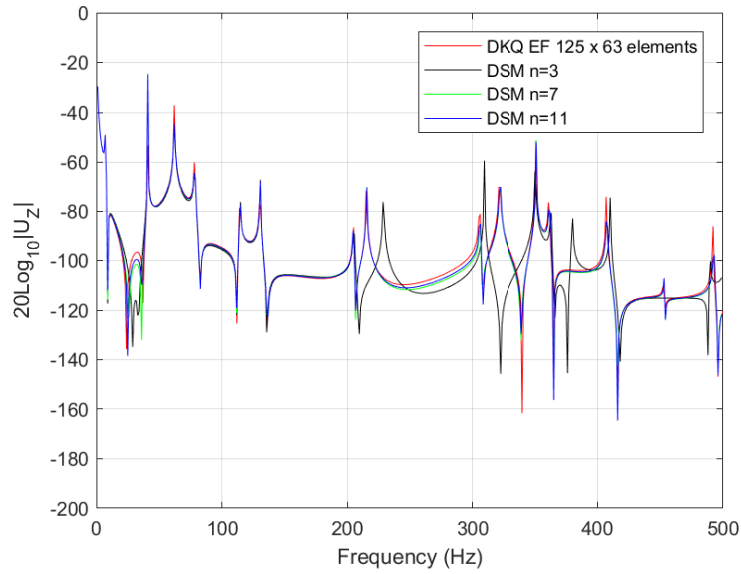


Figure 5: Harmonic response to a symmetrical-symmetrical load

5.2.2. *Antisymmetrical-symmetrical loading*

The structure was subjected to two unit opposite harmonic forces distributed along the edges of the plate defined by $y = b$ and $y = -b$. The loading is shown in Figure 6 and is described by the following components on the Hilbert basis:

$${}^2_3F_0 = 1 \text{ and } {}^4_5F_0 = -1.$$

1
2
3
4
5
6
7
8
9
10
11
12
13
14
15
16
17
18
19
20
21
22
23
24
25
26
27
28
29
30
31
32
33
34
35
36
37
38
39
40
41
42
43
44
45
46
47
48
49
50
51
52
53
54
55
56
57
58
59
60
61
62
63
64
65

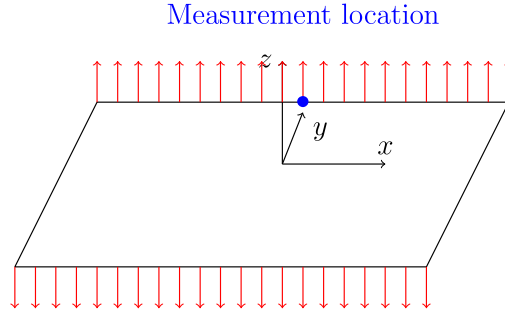


Figure 6: Antisymmetrical-symmetrical loading

The harmonic response of the plate was evaluated at the point located at $x = 0$ and $y = b$ on edge 2 according to the Hilbert basis given in Eq. 42.

395

$$W(a, b) = {}_S^2W_0 + \sum_{n=1}^N {}_S^2W_n \quad (55)$$

The response obtained by DSM for $n = 11$ terms in series and the response obtained with 100×50 DKQ finite elements up to 500 Hz are shown in Figure 7.

The two methods indicate very good agreement.

400 *5.2.3. Concentrated harmonic unit load*

A completely free orthotropic rectangular plate was subjected to a unit vertical harmonic force at the point located at $y = b$ and $x = 0$. The projections of this unit load on the functional basis are evaluated using Eq. 39 to obtain ${}_S^2F_0 = \frac{1}{2a}$ and ${}_S^2F_n = {}_A^2F_n = \frac{1}{a}$. This load case is shown in Figure 8.

1
2
3
4
5
6
7
8
9
10
11
12
13
14
15
16
17
18
19
20
21
22
23
24
25
26
27
28
29
30
31
32
33
34
35
36
37
38
39
40
41
42
43
44
45
46
47
48
49
50
51
52
53
54
55
56
57
58
59
60
61
62
63
64
65

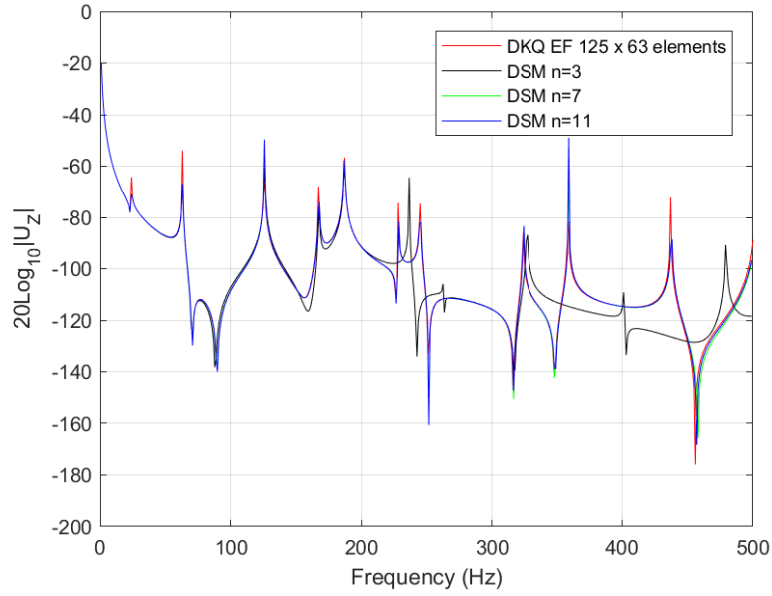


Figure 7: Harmonic response of the plate to an antisymmetrical-symmetrical load

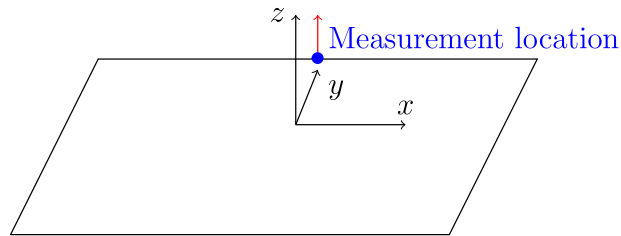


Figure 8: Concentrated load

405

1
2
3
4
5
6
7
8
9
10
11
12
13
14
15
16
17
18
19
20
21
22
23
24
25
26
27
28
29
30
31
32
33
34
35
36
37
38
39
40
41
42
43
44
45
46
47
48
49
50
51
52
53
54
55
56
57
58
59
60
61
62
63
64
65

The harmonic response of the plate was evaluated at the point located at $x = 0$ and $y = b$ on edge 2 according to the Hilbert basis given in Eq. 42.

$$W(0, b) = \frac{2}{S}W_0 + \sum_{n=1}^N \frac{2}{S}W_n \quad (56)$$

The response obtained by DSM for $n = 11$ terms in series and the response obtained with 100×50 DKQ finite elements up to 500 Hz are shown in Figure 9.

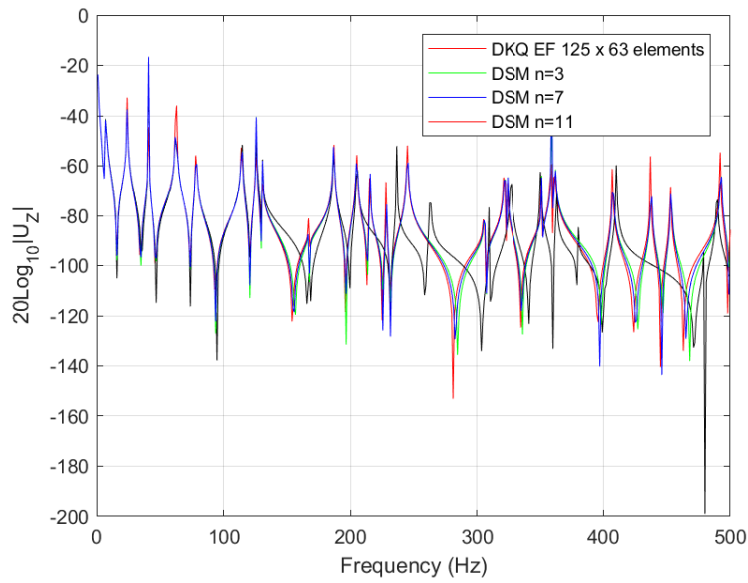


Figure 9: Harmonic response to a harmonic concentrated load

1
2
3
4
5
6
7
8
9
10
11
12
13
14
15
16
17
18
19
20
21
22
23
24
25
26
27
28
29
30
31
32
33
34
35
36
37
38
39
40
41
42
43
44
45
46
47
48
49
50
51
52
53
54
55
56
57
58
59
60
61
62
63
64
65

In a same manner as previous DSM formulations, the DSM based on the new Lévy series obtains high-accuracy harmonic responses despite an extremely low memory cost; the required memory allocation for this DSM is considerably lesser than that for equivalent FE models. The second advantage of this method is CPU consumption time. Table 6 lists the CPU times required to obtain the harmonic response curves. The responses for 500 discrete frequencies were processed. This time depends only on the number n of the terms in Lévy's series.

Table 6: CPU consuming times (500 processed frequencies) and CPU times/frequency

n (DSM)	3	5	7	9	11
CPU times (500 processed frequencies)	1 s	5 s	13 s	27 s	42 s
CPU times (1 processed frequency)	2 ms	10 ms	26 ms	54 ms	84 ms

For comparison, the calculation time for a 125×63 shell FE model, wherein equivalent accuracy is obtained for $n = 11$, is approximately 7 s per processed frequency (via the direct response method).

6. Concluding remarks

The proposed approach is general enough to describe the exact solution for the harmonic response of FFFF plates without using a superposition method. This simplifies the processing of the dynamic stiffness matrix for rectangular plates; four series were used instead of eight. The classical advantages of the DSM over the FEM are preserved: accuracy with truncated series, reduced calculation time, and limited memory allocation.

1
2
3
4
5
6
7
8
9
10
11
12
13
14
15
16
17
18
19
20
21
22
23
24
25
26
27
28
29
30
31
32
33
34
35
36
37
38
39
40
41
42
43
44
45
46
47
48
49
50
51
52
53
54
55
56
57
58
59
60
61
62
63
64
65

The main advantage of these series is that they don't necessitate a symmetry decomposition of the displacement solution. This advantage will allow to address more general dynamic stiffness formulations such as non-symmetric plate or any orthotropic directions. These problems will be the subject of next papers.

The natural frequencies of FFFF rectangular plates were calculated using the proposed DSM. Comparison of these frequencies with those obtained by FEM showed that the average difference between DSM and DKQ formulations is practically negligible. In addition, using the proposed Lévy series, the mode shapes or the displacement field at any circular frequency can be easily processed. In exploring the performances of different Lévy series, the authors noticed that a modal analysis is not adequate without a harmonic response analysis for validation. Series provide fast convergence toward eigenfrequencies but are unable to evaluate the response of the plate at any frequency with few terms.

References

[1] R. Clough, J. Penzien, Dynamics of Structures, McGraw-Hill, New-York, 1975.

[2] U. Lee, Spectral Element Method in Structural Dynamics, Wiley, Singapore, 2009.

[3] T. Richard, Y. Leung, An accurate method in structural vibration analysis, Journal of Sound and Vibration 55-3 (1977) 363-376.

1
2
3
4
5
6
7
8
9
10
11
12
13
14
15
16
17
18
19
20
21
22
23
24
25
26
27
28
29
30
31
32
33
34
35
36
37
38
39
40
41
42
43
44
45
46
47
48
49
50
51
52
53
54
55
56
57
58
59
60
61
62
63
64
65

- [4] R. Lunden, B. Akesson, Damped second-order rayleigh-timoshenko beam
455 vibration in space - an exact complex dynamic member stiffness matrix,
International Journal for Numerical Methods in Engineering 19-3 (1983)
431-449. doi:10.1002/nme.1620190310.
- [5] J. Banerjee, Coupled bending-torsional dynamic stiffness matrix for beam
elements, International Journal for Numerical Methods in Engineering 28
460 (1989) 1283-1289. doi:10.1002/nme.1620280605.
- [6] J. Banerjee, S. Guo, W. Howson, Exact dynamic stiffness matrix of a
bending-torsion coupled beam including warping, Computers and Structures
59(4) (1996) 613-621. doi:10.1016/0045-7949(95)00307-X.
- [7] J. Banerjee, Free vibration of axially loaded composite timoshenko beams
465 using the dynamic stiffness matrix method, Computers and Structures 69
(1998) 197-208. doi:10.1016/S0045-7949(98)00114-X.
- [8] J. Banerjee, Dynamic stiffness formulation and free vibration analysis of
centrifugally stiffened timoshenko beams, Journal of Sound and Vibration
247-1 (2001) 97-115. doi:10.1006/jsvi.2001.3716.
- 470 [9] J. Casimir, T. Vinh, C. Dufort, Dynamic behaviour of structures in large
frequency range by continuous element methods, Journal of Sound and
Vibration 267 (2003) 1085-1106. doi:10.1016/S0022-460X(02)01533-X.
- [10] T. Kim, U. Lee, Exact frequency-domain spectral element model for the
transverse vibration of a rectangular kirchhoff plate, Journal of Sound and

1
2
3
4
5
6
7
8
9
10
11
12
13
14
15
16
17
18
19
20
21
22
23
24
25
26
27
28
29
30
31
32
33
34
35
36
37
38
39
40
41
42
43
44
45
46
47
48
49
50
51
52
53
54
55
56
57
58
59
60
61
62
63
64
65

- 475 Vibration 492 (2021) 1–29. doi:<https://doi.org/10.1016/j.jsv.2020.115812>.
- [11] R. Langley, Application of the dynamic stiffness method to the free and forced vibrations of aircraft panels, *Journal of Sound and Vibration* 135(2) (1989) 319–331.
- 480 [12] A. Leung, *Dynamic stiffness and substructures*, Springer-Verlag, 1993.
- [13] A. Bercin, Analysis of orthotropic plate structures by the direct-dynamic stiffness method, *Mechanics Research Communications* 22(5) (1995) 461–466.
- [14] A. Bercin, R. Langley, Application of the dynamic stiffness technique to the in-plane vibrations of plate structures, *Computers and Structures* 59(5) (1996) 869–875.
- 485 [15] A. Leung, W. Zhou, Dynamic stiffness analysis of laminated composite plates, *Thin-Walled Structures* 25(2) (1996) 109–133.
- [16] A. Leissa, *Vibration of plates*, Nasa-SP160, 1969.
- 490 [17] A. Leissa, The free vibration of rectangular plates, *Journal of Sound and Vibration* 31(3) (1973) 257–293.
- [18] D. Gorman, Free vibration analysis of the completely free rectangular plate by the method of superposition, *Journal of Sound and Vibration* 57-3 (1978) 437–447.

1
2
3
4
5
6
7
8
9
10
11
12
13
14
15
16
17
18
19
20
21
22
23
24
25
26
27
28
29
30
31
32
33
34
35
36
37
38
39
40
41
42
43
44
45
46
47
48
49
50
51
52
53
54
55
56
57
58
59
60
61
62
63
64
65

- 495 [19] J. Casimir, S. Kevorkian, T. Vinh, The dynamic stiffness matrix of two-dimensional elements: application to kirchhoff's plate continuous elements, *Journal of Sound and Vibration* 287 (2005) 571–689. doi:doi:10.1016/j.jsv.2004.11.013.
- [20] M. Boscolo, J. Banerjee, Dynamic stiffness elements and their applications for plates using first order shear deformation theory, *Computers and Structures* 89 (2011) 395–410. doi:doi:10.1016/j.compstruc.2010.11.005.
- [21] M. Boscolo, J. Banerjee, Dynamic stiffness method for exact inplane free vibration analysis of plates and plate assemblies, *Journal of Sound and Vibration* 330 (2011) 2928–2936. doi:doi:10.1016/j.jsv.2010.12.022.
- 505 [22] M. Boscolo, J. Banerjee, Dynamic stiffness formulation for composite mindlin plates for exact modal analysis of structures. part i: Theory, *Computers and Structures* 96-97 (2012) 61–73. doi:doi:10.1016/j.compstruc.2012.01.002.
- [23] M. Boscolo, J. Banerjee, Dynamic stiffness formulation for composite mindlin plates for exact modal analysis of structures. part i: Results and applications, *Computers and Structures* 96-97 (2012) 74–83. doi:doi:10.1016/j.compstruc.2012.01.003.
- 510 [24] F. Fazzolari, M. Boscolo, J. Banerjee, An exact dynamic stiffness element using a higher order shear deformation theory for free vibration analysis of composite plate assemblies, *Composite Structures* 96 (2013) 262–278. doi:http://dx.doi.org/10.1016/j.compstruct.2012.08.033.

1
2
3
4
5
6
7
8
9
10
11
12
13
14
15
16
17
18
19
20
21
22
23
24
25
26
27
28
29
30
31
32
33
34
35
36
37
38
39
40
41
42
43
44
45
46
47
48
49
50
51
52
53
54
55
56
57
58
59
60
61
62
63
64
65

- [25] J. Banerjee, X. S.O. Papkov and, D.Kennedy, Dynamic stiffness matrix of a rectangular plate for the general case, *Journal of Sound and Vibration* 342 (2015) 177–199. doi:<http://dx.doi.org/10.1016/j.jsv.2014.12.031>.
- 520 [26] M. Nefovska-Danilović, M. Petronijević, In-plane free vibration and re-
sponse analysis of isotropic rectangular plates using the dynamic stiff-
ness method, *Computers and Structures* 152 (2015) 82–95. doi:<http://dx.doi.org/10.1016/j.compstruc.2015.02.001>.
- [27] N. Kolarević, M. Nefovska-Danilović, M. Petronijević, Dynamic stiffness
525 elements for free vibration analysis of rectangular mindlin plate assemblies,
Journal of Sound and Vibration 359 (2015) 84–106. doi:<http://dx.doi.org/10.1016/j.jsv.2015.06.031>.
- [28] O. Ghorbel, J. Casimir, L. Hammami, I.Tawfiq, M.Haddar, Dynamic stiff-
ness formulation for free orthotropic plates, *Journal of Sound and Vibration*
530 346 (2015) 361–375. doi:<http://dx.doi.org/10.1016/j.jsv.2015.02.020>.
- [29] O. Ghorbel, J. Casimir, L. Hammami, I.Tawfiq, M.Haddar, In-plane dy-
namic stiffness matrix for a free orthotropic plate, *Journal of Sound and*
Vibration 364 (2016) 234–246. doi:[http://dx.doi.org/10.1016/j.jsv.](http://dx.doi.org/10.1016/j.jsv.2015.11.028)
535 [2015.11.028](http://dx.doi.org/10.1016/j.jsv.2015.11.028).
- [30] N. Kolarević, M. Marjanović, M. Nefovska-Danilović, M. Petronijević, Free
vibration analysis of plate assemblies using the dynamic stiffness method
based on the higher order shear deformation theory, *Journal of Sound and*

1
2
3
4
5
6
7
8
9
10
11
12
13
14
15
16
17
18
19
20
21
22
23
24
25
26
27
28
29
30
31
32
33
34
35
36
37
38
39
40
41
42
43
44
45
46
47
48
49
50
51
52
53
54
55
56
57
58
59
60
61
62
63
64
65

- Vibration 364 (2016) 110–132. doi:<http://dx.doi.org/10.1016/j.jsv.2015.11.016>.
- 540 2015.11.016.
- [31] M. Marjanović, N. Kolarević, M. Nefovska-Danilović, M. Petronijević, Free vibration study of sandwich plates using a family of novel shear deformable dynamic stiffness elements: limitations and comparison with the finite element solutions, *Thin-Walled Structures* 107 (2016) 678–694. doi:<http://dx.doi.org/10.1016/j.tws.2016.08.002>.
- 545 doi:<http://dx.doi.org/10.1016/j.tws.2016.08.002>.
- [32] E. Damjanović, M. Nefovska-Danilović, M. Petronijević, M. Marjanović, Application of the dynamic stiffness method in the vibration analysis of stiffened composite plates, *Procedia Engineering* 199 (2017) 224–229. doi: [10.1016/j.proeng.2017.09.005](http://dx.doi.org/10.1016/j.proeng.2017.09.005).
- [33] E. Damjanović, M. Marjanović, M. Nefovska-Danilović, Free vibration analysis of stiffened and cracked laminated composite plate assemblies using shear-deformable dynamic stiffness elements, *Composite Structures* 180 (2017) 723–740. doi:<http://dx.doi.org/10.1016/j.compstruct.2017.08.038>.
- 550 08.038.
- [34] M. Nefovska-Danilović, N. Kolarević, M. Marjanović, M. Petronijević, Shear deformable dynamic stiffness elements for a free vibration analysis of composite plate assemblies - part i: Theory, *Composite Structures* 159 (2017) 728–744. doi:<http://dx.doi.org/10.1016/j.compstruct.2016.09.022>.
- 555 09.022.
- [35] M. Marjanović, N. Kolarević, M. Nefovska-Danilović, M. Petronijević,
- 560

1
2
3
4
5
6
7
8
9
10
11
12
13
14
15
16
17
18
19
20
21
22
23
24
25
26
27
28
29
30
31
32
33
34
35
36
37
38
39
40
41
42
43
44
45
46
47
48
49
50
51
52
53
54
55
56
57
58
59
60
61
62
63
64
65

Shear deformable dynamic stiffness elements for a free vibration analysis of composite plate assemblies - part ii: Numerical examples, *Composite Structures* 159 (2017) 184–196. doi:<http://dx.doi.org/10.1016/j.compstruct.2016.09.023>.

565 [36] S. Kumar, V. Ranjan, P. Jana, Free vibration analysis of thin functionally graded rectangular plates using the dynamic stiffness method, *Composite Structures* 197 (2018) 39–53. doi:<https://doi.org/10.1016/j.compstruct.2018.04.085>.

[37] S. Kumar, P. Jana, Application of dynamic stiffness method for accurate free vibration analysis of sigmoid and exponential functionally graded rectangular plates, *International Journal of Mechanical Science* 163 (2010). doi:<https://doi.org/10.1016/j.ijmecsci.2019.105105>.

[38] S. Papkov, J. Banerjee, Dynamic stiffness formulation and free vibration analysis of specially orthotropic mindlin plates with arbitrary boundary conditions, *Journal of Sound and Vibration* 458 (2019) 522–543. doi:<https://doi.org/10.1016/j.jsv.2019.06.028>.

[39] Z. Wei, X. Yin, S. Yu, W. Wu, Dynamic stiffness formulation for transverse and in-plane vibration of rectangular plates with arbitrary boundary conditions based on a generalized superposition method, *International Journal of Mechanics and Materials in Design* 17 (2021) 119–135. doi:<https://doi.org/10.1007/s10999-020-09515-9>.

[40] W. Wittrick, F. Williams, A general algorithm for computing natural

1
2
3
4
5
6
7
8
9
10
11
12
13
14
15
16
17
18
19
20
21
22
23
24
25
26
27
28
29
30
31
32
33
34
35
36
37
38
39
40
41
42
43
44
45
46
47
48
49
50
51
52
53
54
55
56
57
58
59
60
61
62
63
64
65

frequencies of elastic structures, *The Quarterly Journal of Mechanics and Applied Mathematics* 24(3) (1971) 263–284. doi:<https://doi.org/10.1093/qjmam/24.3.263>.

[41] W. Wittrick, F. Williams, Buckling and vibration of anisotropic or isotropic plate assemblies under combined loadings, *International Journal of Mechanical Sciences* 16(4) (1974) 209–239. doi:[https://doi.org/10.1016/0020-7403\(74\)90069-1](https://doi.org/10.1016/0020-7403(74)90069-1).

Highlights :

- . We present new Lévy series for calculating the dynamic stiffness matrix of free orthotropic plates.
- . Free boundary conditions are required for plate assemblies.
- . Modal analysis and harmonic analysis are presented.
- . The numerical validation is achieved thanks to comparisons with FE results.

Author Statement :

Karima KHLIFI: Conceptualization, Software, Writing **Jean-Baptiste CASIMIR:** Methodology, Supervision, Review and Editing, **Ali AKROUT:** Supervision, **Mohamed HADDAR:** Supervision, Project Administration

Declaration of interests

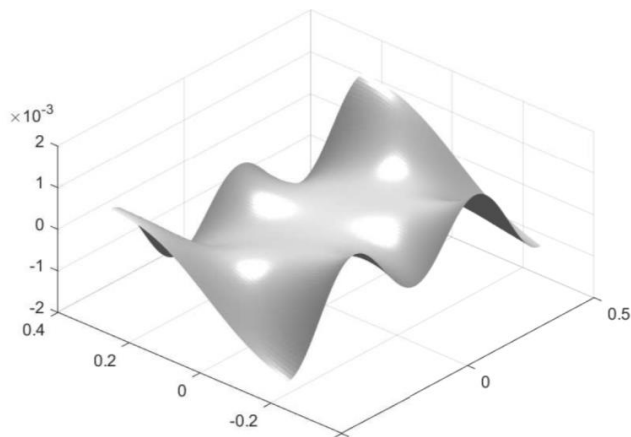
The authors declare that they have no known competing financial interests or personal relationships that could have appeared to influence the work reported in this paper.

The authors declare the following financial interests/personal relationships which may be considered as potential competing interests:

Graphical Abstract

A novel Lévy series for developing a dynamic stiffness matrix for a completely free orthotropic Kirchhoff plate is presented in this paper. The bending behavior is based on the Kirchhoff-Love thin-plate theory. The dynamic stiffness matrix is derived using the new Lévy series without classical symmetry decomposition, simplifying the building procedure. Harmonic responses obtained by this method and the finite element method are compared to establish the rate of convergence and the degree of precision of the current formulation.

A meshless approach :



Harmonic response :

